F I N A L R E P O R T

Reduction and Analysis of Data From Cosmic Dust Experiments on Mariner IV, OGO III, and Lunar Explorer 35

NASA Research Grant NGR 39 - 012 - 001

Temple University

Philadelphia, Pennsylvania

June 1974

TABLE OF CONTENTS

I. Introduction

The work under this NASA grant has been primarily concerned with the analysis of data from the cosmic dust experiment on three NASA missions. These missions were Mariner IV, OGO III, and Lunar Explorer 35. The analysis effort has included some work in the laboratory of the physics of microparticle hypervelocity impact. This laboratory effort was initially aimed at the calibration and measurements of the different sensors being used in the experiment. The later effort was conducted in order to better understand the velocity and mass distributions of the picogram sized ejecta particles.

Much of the data analysis has been previously reported in a list of papers and publications covering this work as found in Appendix II. The laboratory work regarding calibrations that is not covered in previous reports has been reported in prior grant progress reports. The new laboratory effort and theoretical studies which are unpublished, but being prepared for publication, are found in this final report. In addition, the recent papers summing the Lunar Explorer 35 data and a continuing consideration of the Mariner IV data are also included in the report.

II. Lunar Explorer 35

A. The Lunar Explorer 35 spacecraft was launched in June 1967. The achieved lunar orbit had an initial aposelene of 9385 km and periselene of 2536 km. One of the experiments on the LE 35 was a cosmic dust experiment. The experiment conducted measurements of the flux of dust particles in selenocentric space. The results of these measurements have been reported in several papers (all listed in the project references: Appendix II). The two papers which follow in section IIC are the summary papers for the LE 35 work up to the present time. Section II B presents a brief description of the experiment instrumentation in order to facillitate the understanding of the data papers.

B. The LE 35 dust particle experiment contained two independent sensor arrays. A functional sketch of the instrument is seen in figure IIB-1. The large area circular detector contains two sensors: (1) an acoustical ceramic transducer bonded to the plate, and (2) a large area capacitor sensor deposited on the impact side of the impact plate. A dust particle colliding with the impact plate produces an acoustical wave which is detected by the ceramic transducer. The resulting signal from this sensor is pulse height analyzed and the event data stored in the electronic instrumentation. Results of hypervelocity calibration studies related to the Lunar Explorer 35 dust particle experiment showed the nominal mass threshold sensitivity of this sensor to be 5 picograms. When the capacitor sensor's dielectric is penetrated by a dust particle, an electrical signal occurs which is also analyzed and the information stored in the electronic data system. The mass threshold sensitivity for this sensor is nominally 100 picograms. Logic circuitry in the instrumentation detects the coincident signals from two sensors, and this information is also stored. The second sensor array is a tubular detector containing three sensors. The entrance of the tube is a very thin film. When a dust particle with velocity greater than

5 km/sec passes through the film, a plasma is produced which can be detected. After the particle traverses the tube, it impacts on the diaphragm of a capacitor microphone. Plasma is again produced and detected. The time of flight of the particle in the tube is determined from these two plasma-produced pulses. The capacitor microphone gives an electrical signal directly related to the impulse delivered to the diaphragm by the impacting particle. The data from these sensor signals are also stored in the experimen data system along with the appropriate logic information concerning validity of the data. In addition, the experiment instrumentation contains circuits designed to detect electromagnetic and electrostatic noise transients to aid in further evaluation of the validity of the data.

A more detailed discussion of the electronic logic and data handling is found in Appendix I.

C. Data Analysis from papers presented at the XIV and XV COSPAR meetings follow:

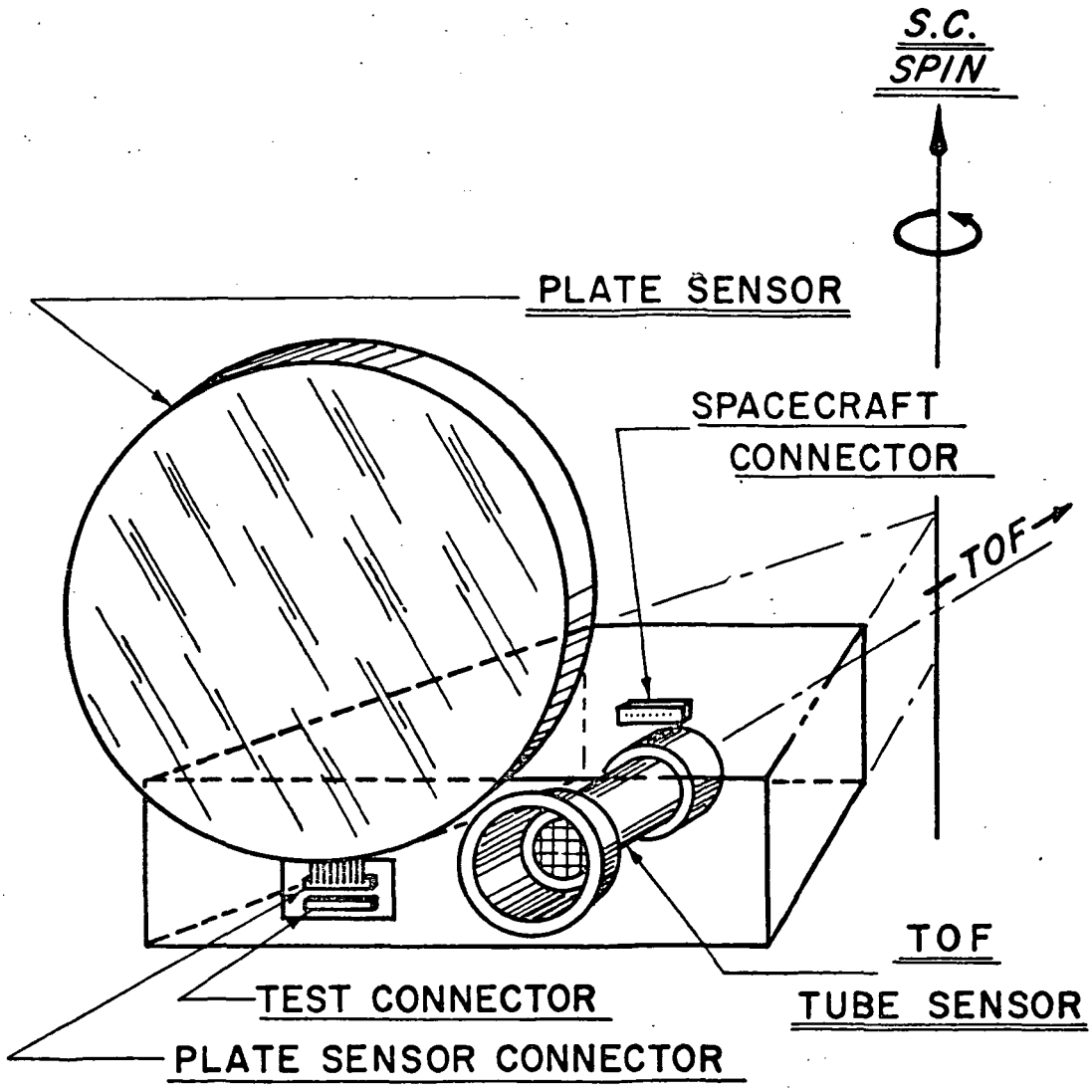

FIGURE IIB-IV

Space Research XII, Akademie-Verlag, Berlin, 1972

Pub #23

IIC1

LUNAR EXPLORER 35: 1970 DUST PARTICLE DATA and ANALYSIS of SHOWER RELATED PICOGRAM LUNAR EJECTA ORBITS in the EARTH-MOON SYSTEM

W. M. Alexander (Baylor University, Waco, Texas), C. W. Arthur (UCLA, Los Angeles, California, USA), J. Lloyd Bohn (Temple University, Philadelphia, Pennsylvania, USA), J. H. Johnson (Advanced Technology Center, Inc., Grand Prairie, Texas, USA), B. J. Farmer (Advanced Technology, Inc., Grand Prairie, Texas, USA).

ABSTRACT: The Lunar Explorer 35 dust particle experiment measurement has determined the mean sporadic flux in selenocentric space for the period July 1967 - July 1970 to be $2.5 \pm 1.8 \times 10^{-4}$ p $m^{-2}s^{-1}(2\pi\ sr)^{-1}$ with fluctuations of an order of magnitude during major meteor showers. The experiment datum during the 12 month period commencing with June 1969, shows, for the 3rd year, coincident increase of flux during the major meteor showers. Orbit calculations for picogram ejecta particles escaping the moon, indicate orbit patterns in cislunar space which vary annually. Detection of lunar ejecta microparticles related to primary shower particles traversing the earth's sphere of influence is significantly modulated by the annual position of the earth, moon, and streams. One increase in an OGO III flux period shows a possible correlation between the rates measured from Lunar Explorer 35 during the Perseid shower in 1967. For the Geminids, a significant number of ejecta orbits passed through the earth's sphere of influence in 1967, very few in 1968-1969, and only a moderate amount in 1970. The Radiation Meteoroid Satellite experiment may have detected a lunar ejecta particle related to the Geminid shower primary particles. The satellite may also have detected a lunar ejecta particle related to the 1970 Ursid shower primary particles. The orbit studies indicate that the latter case was more favorable in December 1970.

4

1. Introduction

Data from the first two years of operation of the Lunar Explorer 35 dust particle experiment has been reported by Alexander, et al [1,2]. The nature of the data has shown a mean flux during non shower periods which was a factor of less than two above that of the flux measured in interplanetary space as reported from Mariner IV and Pioneers 8 and 9 [1,2,3]. However, the flux increased during periods of major meteor showers [2]. For the third year, additional data from Lunar Explorer 35 continues to show a flux increase in selenocentric space during periods of major meteor showers. It is the intention of this paper to present (1) evidence of a third year repeat of flux increase during periods of major meteor showers, and (2) results of orbit studies of picogram lunar ejecta associated with the showers. The Lunar Explorer 35 measurement reveals a mass cutoff of lunar ejecta which escapes the moon for an ejecta mass less than 10^{-10}gm[1]. The orbit studies consider picogram particles ejected by larger shower particles. The results of the study indicate that the relative position of the earth-moon-shower radiant determine the possible significant presence of shower related lunar ejecta in the earth's sphere of influence.

2. Lunar Explorer 35 Dust Particle Experiment

A description of the Lunar Explorer 35 dust particle experiment instrumentation has been published [1]. The experiment contained a large area coincident circular detector and a triple coincident tubular detector. Two sensors comprise the circular detector: an acoustical ceramic transducer bonded to the plate and a large area capacitor sensor deposited on the impact side of the plate. The acoustical signal was produced by the hypervelocity impact of a dust particle on the plate. A pulse height analysis was also performed on the signal received from the ceramic transducer. Hypervelocity calibration studies indicate that the nominal mass threshold of the ceramic sensor was 5 picogram and the capacitor sensor 100 picograms[1,4].

As previously reported [2], the TOF measurements possible from the tubular detector have suffered interference problems with another experiment, and this data is not included at the present time. Twice during a 24 hour period, noise burst due to calibration of another experiment have occurred in the dust particle experiment. The data reported is free from any evidence of noise.

3. DATA

The additional data during periods of non shower activity shows a mean flux of

$$\Phi = 2.5 \pm 1.8 \times 10^{-4} \text{ p m}^{-2}\text{s}^{-1} (2\pi \text{ sr})^{-1}$$

for the three year period July 1967 to July 1970. Data for four major meteor shower periods are shown in Fig. 1. The event rate for the Perseids are given for 1967 and 1969. A six week data gap occurred during the Perseid dates for 1968. Fig. 1 also shows the event rates for the Leonids, Southern Taurids, and Geminids during 1967, 1968 and 1969. The data points are given in events per four day time intervals. The mean background count rate in terms of events per four day periods was about one event per period.

4. Shower Related Lunar Ejecta Orbit Calculations

During the past decade, several studies have been made relating to the orbits of lunar ejecta in the earth-moon system [5,6,7]. In general, the following characteristics have been established:

(a) orbits exist which contain particles impacting on the earth,

(b) orbits exist which contain particles impacting on the moon,

(c) orbits exist for particles being captured by the earth-moon system in long lifetime orbits,

(d) orbits exist for particles being captured by the earth-moon system in short lifetime orbits (a few days to a few years),

(e) for masses of 100 picograms or less, orbits as in (d), but exiting the earth-moon system always in an ani-solar direction.

[6]

In the above considerations, the largest number of particles fall in the category (d). This means that a permanent enhancement of the dust particle flux near the earth resulting from lunar ejecta would not exist.

Today's orbit calculations certainly confirm the earlier results. The purpose of the present studies was to consider the nature of the orbits of only picogram-sized particles ejected from the lunar surface resulting from the hypervelocity impact of a particle in a known major meteor stream.

4.1 The standard equations of motion for a dust particle in the sun-earth-moon gravitational system are shown in fig. 2. The displacement with respect to the earth of a lunar ejecta particle subjected to the gravitational forces of the sun, earth and moon and the solar radiation pressure can be determined from the final final equation. The solutions of interest are those where a known major meteor shower particle impacts the lunar surface. In fig. 3, the pertinent angles for the Geminids are depicted. The angles are with respect to a coordinate system based on 0° being in the anti-solar direction. The angle θ gives the angle of the moon with respect to the earth for a specific time. The angle Φ shows the most probable angle for picogram-sized lunar ejecta. The latter angles result from the characteristics of hypervelocity impact derived from laboratory investigations [5]. The ejecta velocities are always considered to be between 75° and 90° with respect to the shower particle radiant.

4.2 The case of lunar ejecta resulting from primary particles in the Geminid meteor stream is presented in fig. 4 and fig. 5. In fig. 4, orbits of ejecta particles with three different escape velocities, 2.30, 2.35 and 2.40 km s^{-1}, and leaving with an angle Φ of 237°(Geminids,1968) are shown. These particles move towards the earth and then are rapidly removed from the earth-moon system . This position is for Geminids three days prior to maximum flux. As time progresses and the moon moves to larger values of θ, no Geminid ejecta particles come near the earth. This is shown further in fig. 5 with θ of 315°.

All particles leave the earth-moon system in an anti-solar direction and never approach the earth. Conditions for 1967 are presented in fig. 5 with position of the moon given for the beginning and ending of the Geminid period. It is readily seen that ejecta from the lunar surface moves into and through the earth's sphere of influence with a probable impact of some particles on the earth in 1967. Similar studies for 1969 and 1970 show small probability in either year for any Geminid related particles near the earth.

4.3 Studies were also undertaken for periods of the Perseid shower. Figure 6 shows possible orbits at the beginning, peak and ending of the Perseid period in 1967. There should have been no Perseid related particles near the earth until almost the peak of the period. A portion of the particles passed through the earth's sphere of influence between D224 and D227, 1967. Fig. 7 shows what may happen under unique conditions. The type of orbits shown only exist for the few degress of ϕ given. In this case, particles could exist in the earth-moon system for as long as five months.

5. Discussion of Results

The results show that there are years in which the dust particle flux near the earth cannot be enhanced by a particular meteor shower. The solid angle subtended by the earth's sphere of influence with respect to the moon is small, thus the probability of measuring lunar ejecta at the earth, even during periods of possible earth-lunar ejecta intercepts,must remain small. As seen in fig. 7, the orbits were vast with respect to the earth and possible satellite orbits, and thus, any significant impact event rate increase measured by a satellite must be considered very carefully. However, OGO III showed it's highest mean flux during the fall months of 1967 - a factor slightly greater than two over the rest of the valid measurement period.

The Radiation Meteoroid satellite registered two TOF events near the major December showers, and a front film

increase during the second shower, the Ursids. The second event could easily be lunar ejecta as well as primary meteor stream particles.

6. Acknowledgement

The work was partially supported under NASA Research Grant NGR 39 - 012 - 001.

7. References

[1] W. M. Alexander, C. W. Arthur, J. D. Corbin, and J. Lloyd Bohn, XIIthe COSPAR Meeting Prague(1969), Space Research X (North-Holland, Amsterdam,1970)p. 252.

[2] W. M. Alexander, C. W. Arthur, and J. Lloyd Bohn, XIIIth COSPAR Meeting, Leningrad (1970) in print.

[3] O. E. Berg and U. Gerloff, XIIIth COSPAR Meeting, Leningrad (1970) in print.

[4] W. M. Alexander, J. Lloyd Bohn, and A. Wever, Xth COSPAR Meeting, London (1967), preprint.

[5] D. Gault, private communication.

[6] C. W. McCracken, NASA SP-135 p.213-224 (1965).

[7] I. I. Shapiro,D. A. Lautman, G. Colombo, J. GEOPHYS. Res. 71, 5695 (1966).

FIGURE CAPTIONS

Figure 1: Event Rates During Four Meteor Showers 1967 - 1969

Figure 2: Equations of Motion for Dust Particle in Sun-Earth-Moon System

Figure 3: Angles for Meteor Shower Related Lunar Ejecta (Geminids)

Figure 4: Geminid Related Lunar Ejecta Orbits (three escape velocities-1968)

Figure 5: Geminid Related Lunar Ejecta Orbits With Constant Escape Velocity and Varying Ejected Angle (1967 and 1968)

Figure 6: Perseid Related Orbits for Lunar Ejecta (1967)

Figure 7: Special Case of Perseid Related Lunar Ejecta Orbits, 1967

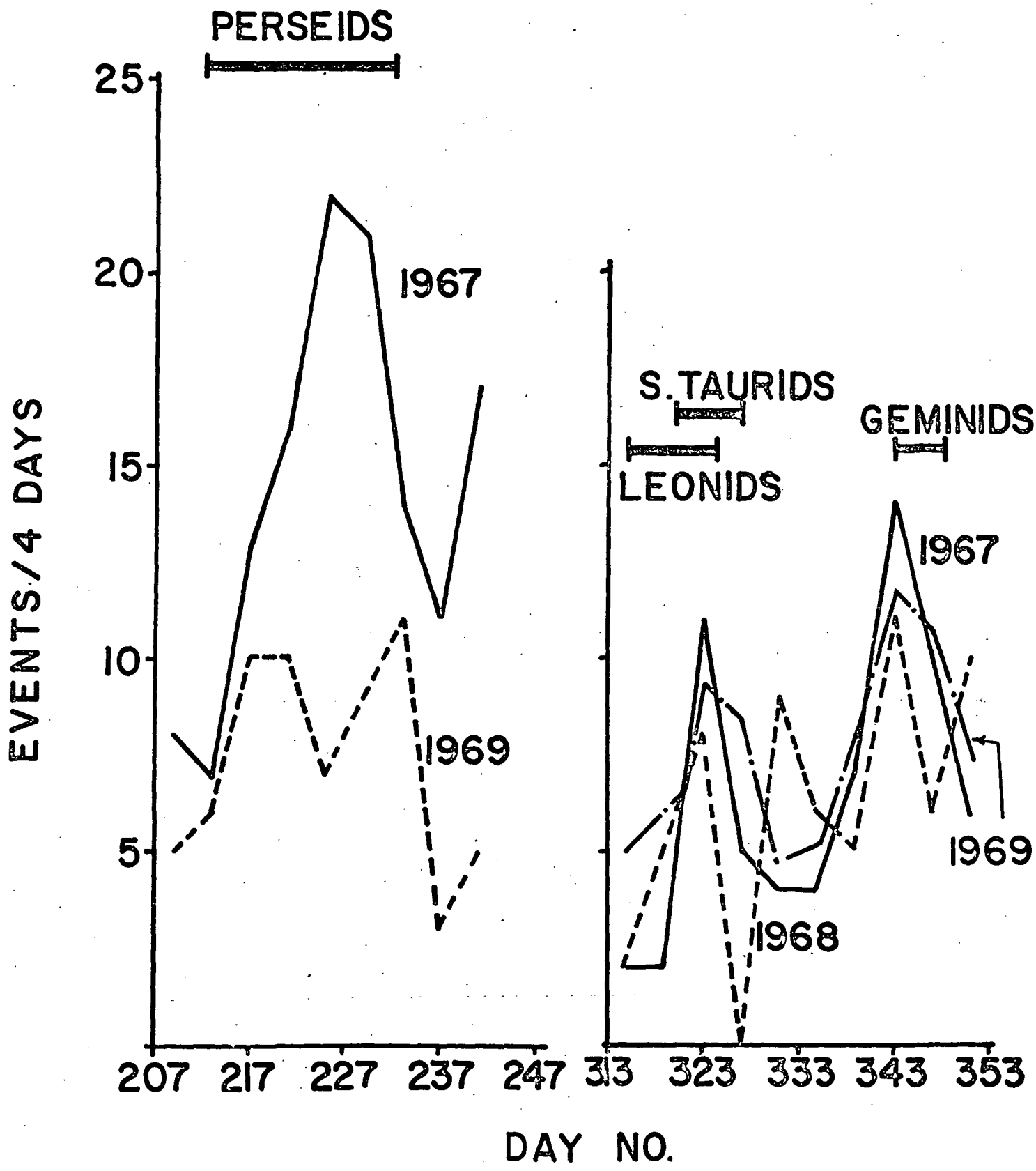
PERSEIDS
25
20
15
10
5
1967
1969
S.TAURIDS
LEONIDS
GEMINIDS
1967
1969
1968
EVENTS/4 DAYS
207
217
227
237
247
313
323
333
343
353
DAY NO.

FIGURE 1

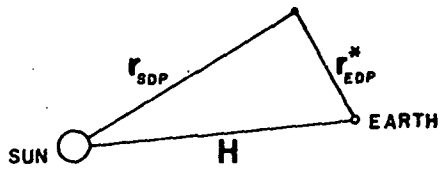

EQUATION OF MOTION FOR DUST PARTICLE RELATIVE TO THE SUN

$$\frac{d^2 r_{SDP}}{dt^2} = \frac{-GM_S r_{SDP}}{r_{SDP}^3} - \frac{GM_E r_{EDP}}{r_{EDP}^3} - \frac{GM_M r_{MDP}}{r_{MDP}^3} + a_{SRP}$$

TRANSFORMING TO THE EARTH – MOON SYSTEM

$$\frac{d^2 r_{SDP}}{dt^2} = \frac{d^{*2} r^*}{dt^2} + \omega_E \times (\omega_E \times r^*) + 2\omega_E \times \frac{d^* r^*}{dt} + \frac{d\omega_E}{dt} \times r^* + \frac{d^2 H}{dt^2}, \text{ and}$$

EQUATION OF MOTION FOR DUST PARTICLE IN EARTH-MOON SYSTEM

$$\frac{d^{*2} r^*_{EDP}}{dt^2} = -\frac{GM_S r_{SDP}}{r_{SDP}^3} - \frac{GM_E r_{EDP}}{r_{EDP}^3} - \frac{GM_M r_{MDP}}{r_{MDP}^3} + a_{SRP} - \omega_E \times (\omega_E \times r^*) - 2\omega_E \times \frac{d^* r^*}{dt} - \frac{d^2 H}{dt^2}$$

where: $a_{SRP} = -a_{GS}$, and $\frac{d^2 H}{dt} = -\frac{GM_S r_{SE}}{r_{SE}^3}$

FIGURE 2

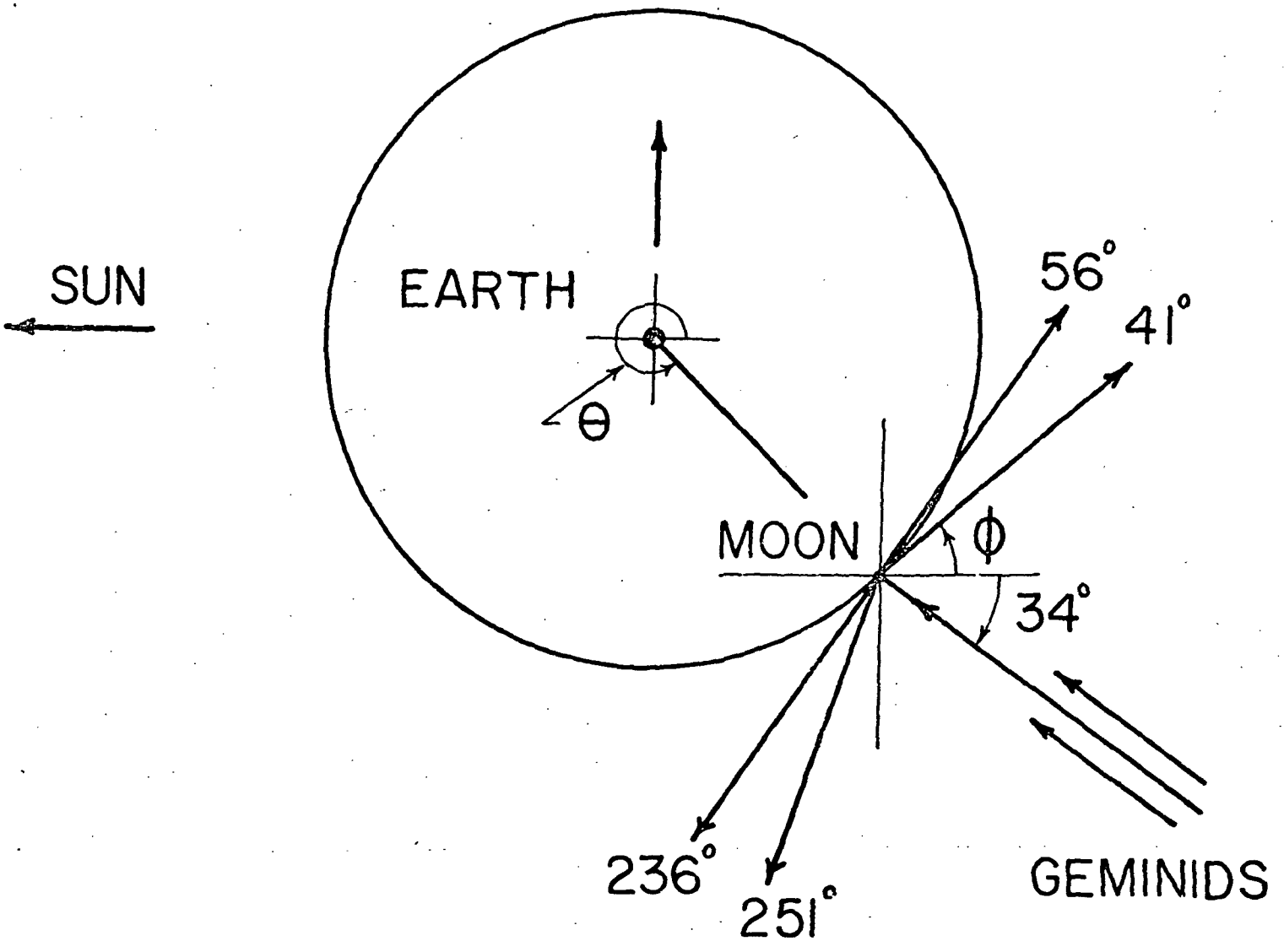

FIGURE 3

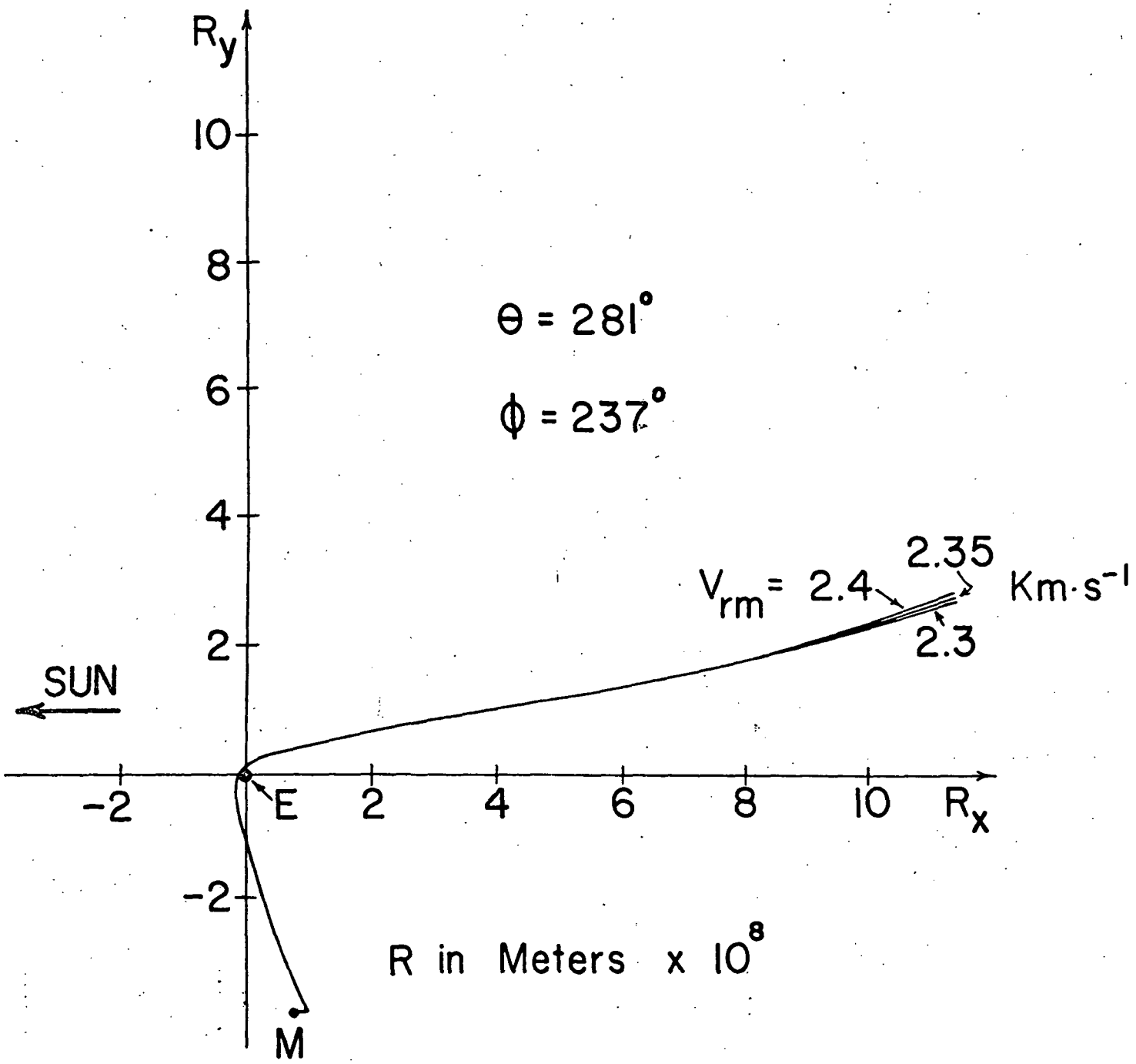
R_y
10
8
6
4
2
-2
-2
2
4
6
8
10
R_x
E
M
SUN
$\theta = 281°$
$\phi = 237°$
V_{rm} = 2.4
2.35
2.3
Km·s^{-1}
R in Meters x 10^8

FIGURE 4

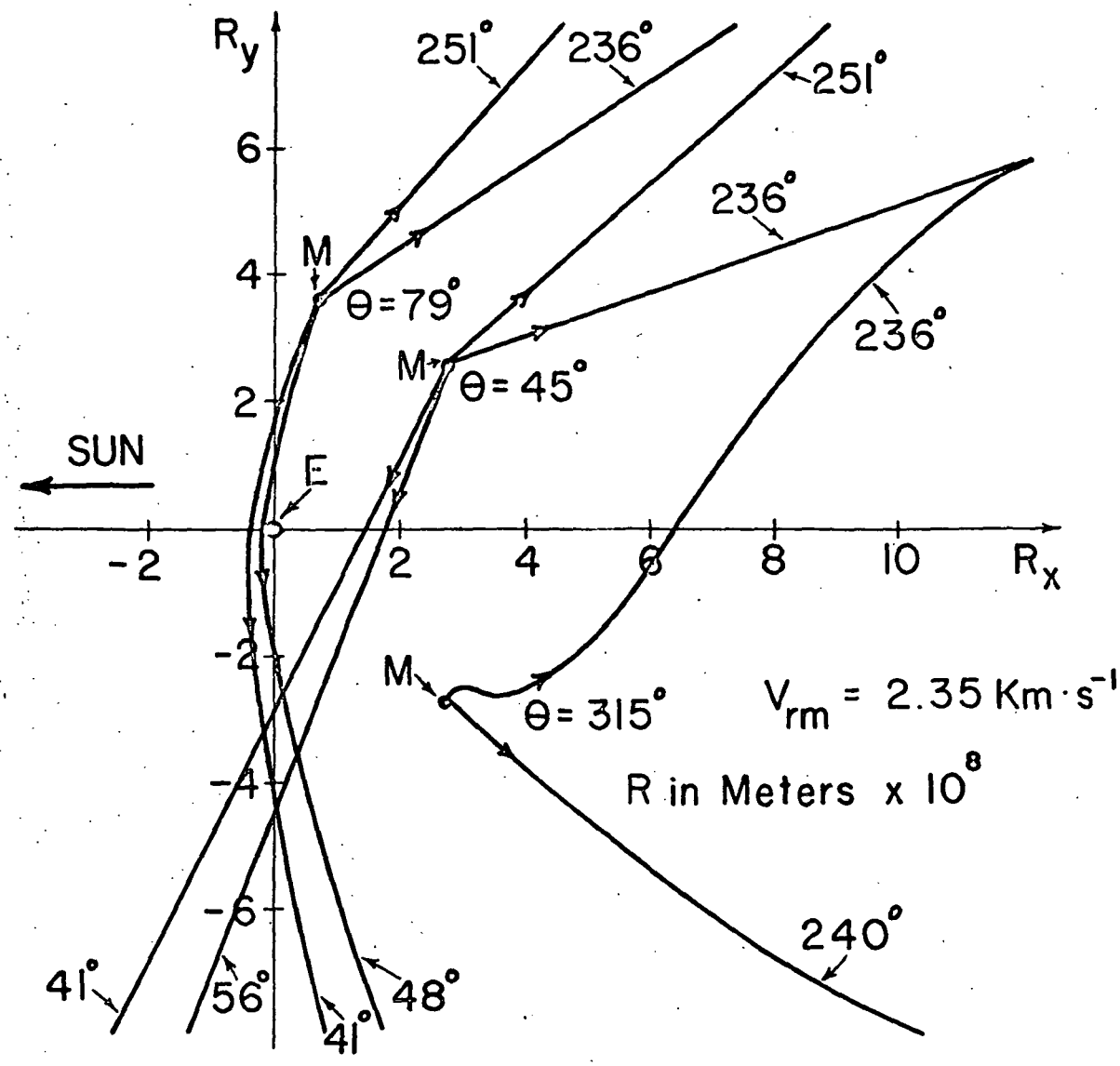
R_y
R_x
SUN
E
M
$\Theta = 79°$
$\Theta = 45°$
$\Theta = 315°$
$V_{rm} = 2.35\ Km \cdot s^{-1}$
R in Meters x 10^8
251°
236°
251°
236°
236°
240°
41°
56°
48°
41°
-2
2
4
6
8
10
-2
-4
-6
4
2
6

FIGURE 5

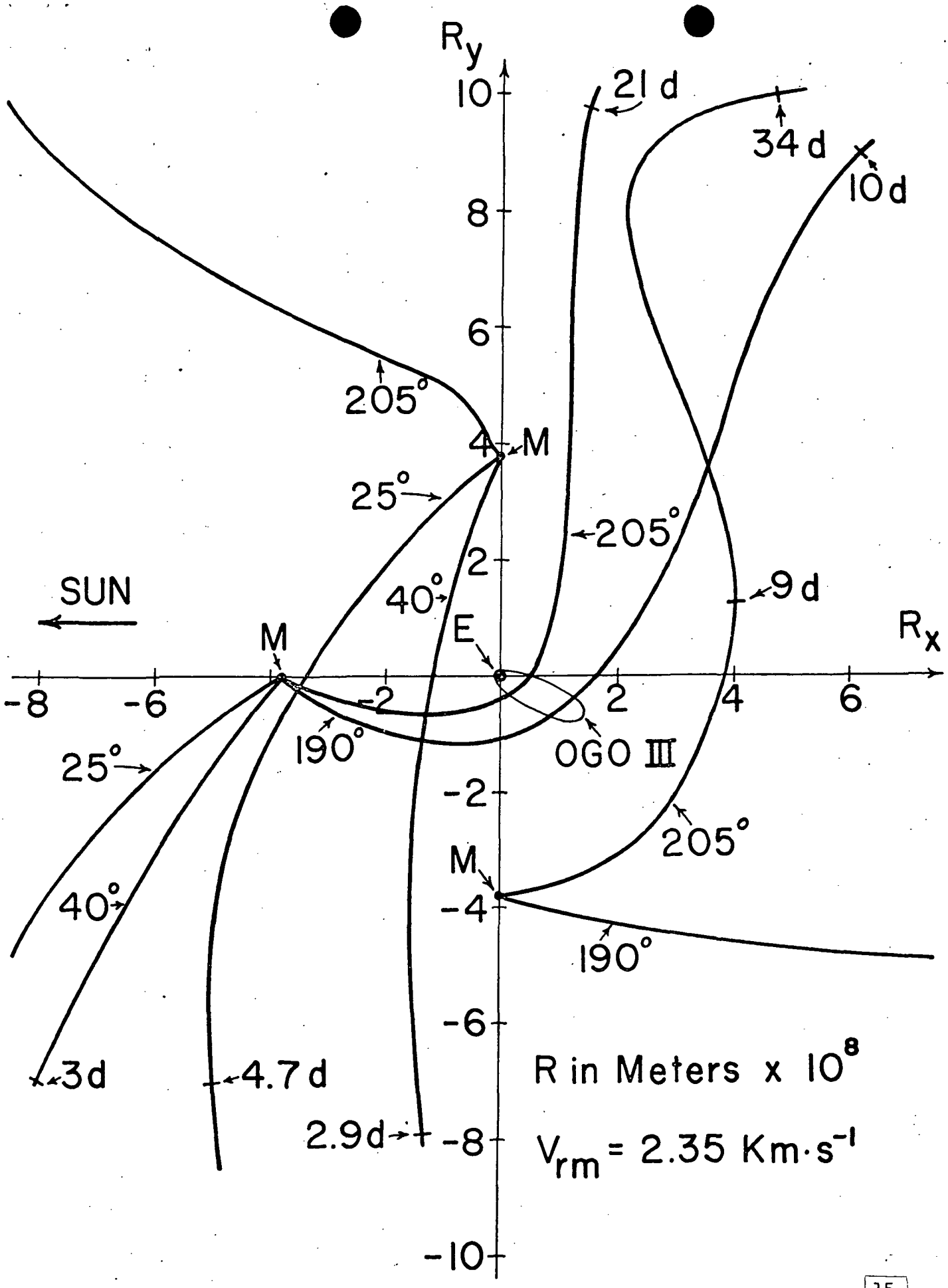
R_y
10
8
6
4
2
-2
-4
-6
-8
-10
21 d
34 d
10 d
9 d
205°
25°
40°
190°
M
E
SUN
R_x
-8
-6
-2
2
4
6
OGO III
3d
4.7 d
2.9d
R in Meters x 10^8
V_{rm} = 2.35 Km·s^{-1}

FIGURE 6

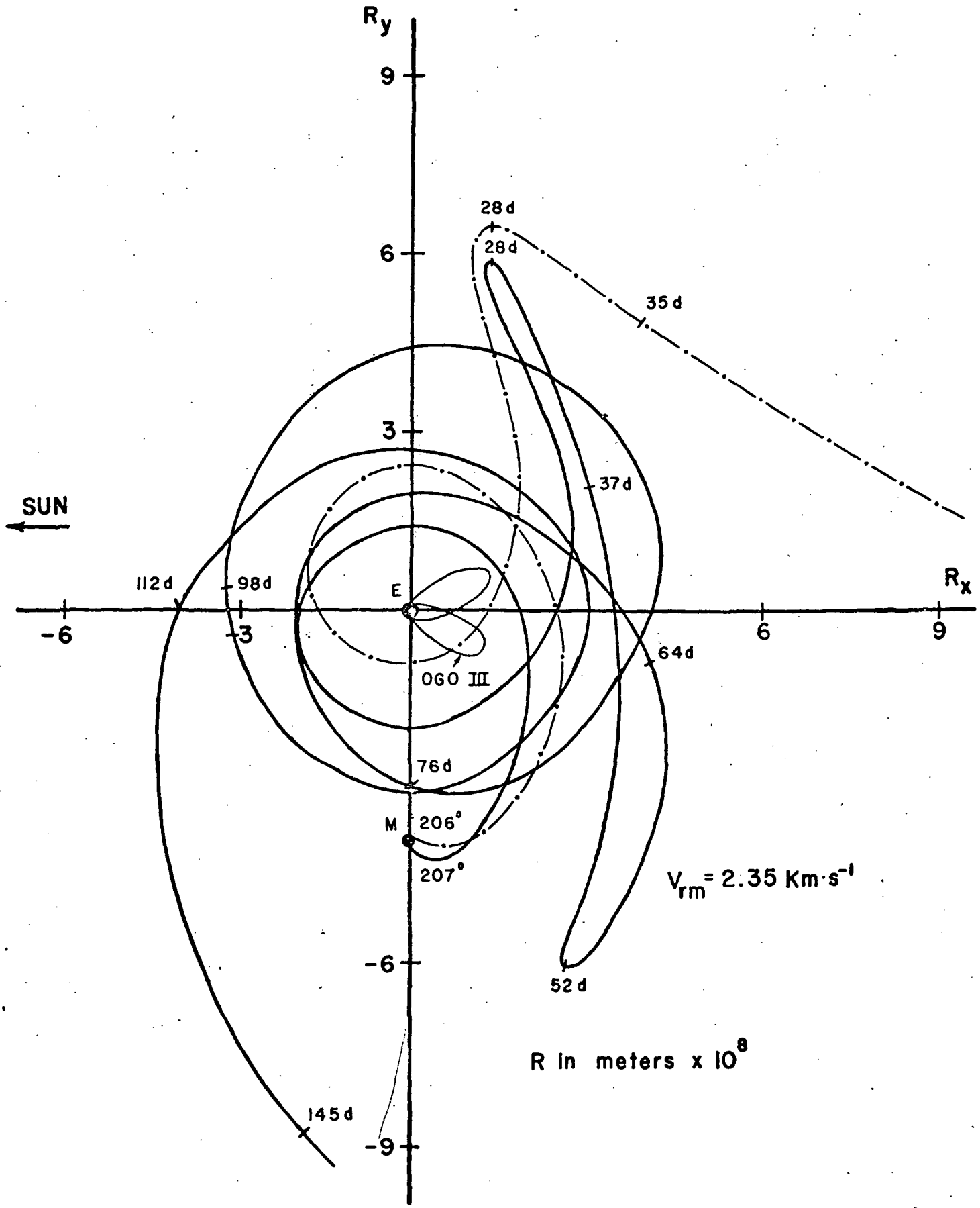
R_y
9
6
3
-6
-9
R_x
-6
-3
6
9
28d
28d
35d
37d
SUN
112d
98d
E
64d
OGO III
76d
M
206°
207°
52d
145d
V_{rm}= 2.35 Km·s^{-1}
R in meters x 10^8

16

FIGURE 7

Space Research XIII, Akademie-Verlag, Berlin, 1973 (Pub. No. 26)

IIC2

FOUR YEARS OF DUST PARTICLE MEASUREMENTS IN CISLUNAR AND SELENOCENTRIC SPACE FROM LUNAR EXPLORER 35 AND OGO III

W. M. Alexander (Baylor University, Waco, Texas, USA), C. W. Arthur (UCLA, Los Angeles, California, USA), J. Lloyd Bohn (Temple University, Philadelphia, USA), J. C. Smith (Baylor University, Waco, Texas, USA).

ABSTRACT: Since July 1967, knowledge concerning the distributions of picogram size particulate matter in selenocentric space has been obtained from the Lunar Explorer 35 dust particle experiment. For almost 40% of the time, the mean sporadic cumulative flux is quite similar to the flux in interplanetary space at $2 \pm 0.8 \times 10^{-4}$ p $(m^2 \text{ sec } 2\pi \text{ sr})^{-1}$. However, there are fluctuations of an order of magnitude during major meteor showers. The coincident increase of the flux in selenocentric space during the shower periods has been observed for the fourth year. The 100 picogram sensor does not show an increase during shower times, indicating a mass threshold of less than 100 picograms for particles with velocities equal to or greater than lunar escape velocity. The flux values from Lunar Explorer 35 are compared to other long lifetime measurements in selenocentric, cislunar and interplanetary space with excellent agreement for masses less than 10^{-9} gm.

1. INTRODUCTION

The initial measurements in selenocentric space were reported by Nazarova [1] and Gurtter and Grew [2]. These measurements were followed by Lunar Explorer 35, which has continued to provide data

since July, 1967. Initial and intermediate reports of the results of the measurement have been made by Alexander et al [3,4,5]. Additional data have been reduced since the last report [5], and further analysis of possible cislunar orbits of picogram particles coming from the lunar surface have provided additiona insight into the possible effects of the minute lunar ejecta. A general review of the complete Lunar Explorer 35 data are given, and a critical examination is presented concerning the role of the lunar data in cumulative flux-mass distribution models.

2. LUNAR EXPLORER 35 DUST PARTICLE EXPERIMENT

A description of the Lunar Explorer 35 dust particle experiment is given in [3,4]. The significant data which have been reported [3,4,5] was obtained from the large area coincidence detector. Two sensors comprise the detector: an acoustical ceramic transducer bonded to a large area circular impact plate, and a large area capacitor sensor deposited on the surface of the impact plate. Calibration studies show that the nominal mass threshold of the acoustical sensor is 5 picograms and the capacitor 100 picograms. Coincident events are detected by logic circuitry in the electronic instrumentation and the information stored in the spacecraft data storage system.

3. DATA FROM THE LUNAR EXPLORER 35 EXPERIMENT

The histogram in fig. 1 depicts the cumulative flux rate for selenocentric space from launch through 1970. The flux is presented in 8 day increments in order to be able to show the complete flux picture obtained from the measurement. Even though using 8 day increments causes considerable smoothing in the data presentation,

the enhancement of the sporadic flux during the periods of major meteor showers is evident. This phenomenon has been reported in preceeding papers [3,4,5], but the fig. 1 histogram represents the first extended presentation showing the extent of the effect.

A more detailed picture is seen in fig. 2 where the number of events (4 day periods) during six of the major meteor showers is shown. The sporadic non-shower rate is about two events per 4 day period, thus, it is seen that a change in flux of an order of magnitude occurs during a significant number of the showers. Also, the repetition each year is quite evident in the good and sometimes excellent agreement between the high event rates obtained from the Lunar Explorer 35 measurements and the shower periods. In comparing the fluxes over the four years, the variations in the maximums determined by the measurements lie well within variations obtained by ground-based data for major meteor streams.

There are several periods of time for which no data are available. The largest data gap occurs during the time of the Perseids in 1968. Hence, one opportunity for studying the shower was missed. There are noise bursts [3] in the data caused by the calibration sequence of another experiment. Elimination of these events from the data still left, in general, 90 - 95 % of each day clear of noise and in no case less than 85 %.

The data presented in figs. 1 and 2 were obtained from the acoustical sensor which has a mass threshold sensitivity of 5 picograms. As previously reported [3], the data rate for the 100 picogram sensitivity threshold sensor is very low with no discernable enhancement of the 100 picogram flux during shower periods. This result has not changed.

4. DISCUSSION OF LUNAR EXPLORER 35 RESULTS

4.1 FLUX DURING NON-SHOWER PERIODS. As seen in fig. 1, there is a general similarity between the data from D071 to D200 each year. The flux is higher in 1969 than in 1968 or 1970. There are spring meteor showers and the flux in 1969 does suggest a possible correlation with two daylight streams and some unnamed southern hemisphere showers [4]. However, when the flux for all three years is determined, it is found to be $2 \pm 0.8 \times 10^{-4}$ p $(m^2 \text{sec } 2\pi \text{ sr})^{-1}$. This value compares quite favorably with that of Mariner IV, Pioneer 8 and 9 from interplanetary space, and OGO III in cislunar space. This flux value is for the 5 picogram particles.

The flux of the 100 picogram particle remains the same as previously reported, 7.4×10^{-6} p $(m^2 \text{sec } 2\pi \text{sr})^{-1}$, and is found to be in excellent agreement with Mariner II and the Lunar Orbiter penetration experiment results [7]. An analysis of the Lunar Explorer 35 data with respect to cumulative flux models is presented in a following section.

For the non-shower periods there is no significant variation of the flux in selenocentric space and that of cislunar or interplanetary space over the mass range, $5 \times 10^{-12} \leq m \leq 1 \times 10^{-9}$ grams.

4.2 5 PICOGRAM FLUX DURING SHOWER PERIODS. The flux enhancement during the periods D(201 -- 071) for four years either represents the presence of picogram particles in the primary meteor streams, or lunar ejecta resulting from the impact at hypervelocities of larger stream particles on the lunar surface.

If the particles are stream particles, they are of recent origin since the radiation pressure and drag perturbing forces remove

picogram size particles from their original orbits in very short periods of time. In addition, the absence of an enhancement of 100 picogram particles suggests a flux-mass distribution in the streams which is drastically different from that of sporadic interplanetary dust particle distributions.

A hypervelocity impact produced ejecta having widely varying masses and velocities. The smallest particles have the highest velocities. The nature of the mass - velocity distributions for the many combinations of impacting particles, impact surfaces and velocities is extremely complex. The efficiency of producing lunar ejecta with escape velocities from meteoroid impacts on the lunar surface is not known, but some idea of the efficiency level is suggested by the Lunar Explorer 35 data if the assumption is made that the enhancement seen for a portion of the year is lunar ejecta. As already stated, there is no significant difference between the flux in selenocentric space and that measured in cislunar space and interplanetary space (near 1 AU) during non-shower periods even though the sporadic meteoroids are impacting the lunar surface with velocities in the hypervelocity range. The enhanced flux appears to be related to streams of relatively high rate and moderate velocities or high rate and high velocities. This indicates that the efficiency of producing picogram particles with escape velocities is low.

4.3 MASS THRESHOLD FOR LUNAR EJECTA ESCAPE VELOCITIES.

As stated above, the nature of the hypervelocity phenomenon on the lunar surface is such that only smaller particles have escape velocity. The enhnacement seen in the Lunar Explorer 35 data for 5 picogram particles and the lack of enhancement for 100 picogram particles

suggests that only particles with masses less than 100 picograms achieve escape velocity. At the present time, the analysis of the data cannot differentiate between lunar ejecta and primary stream particles using the measured data alone. However, the overall evidence indicates that the 5 picogram flux enhancement is the result of lunar ejecta related to primary shower particles.

4.4 ORBIT CONSIDERATIONS OF 5 PICOGRAM LUNAR EJECTA.

Over the past ten years, a number of investigation have been made concerning orbits of lunar ejecta in the earth-moon system [8,9,10]. These have concentrated on searching for conditions which would produce a significant number of long lifetime orbits. Since Lunar Explorer 35 and Lunar Orbiter results do not indicate any consistent lunar ejecta flux for masses greater than 100 picograms, studies of 5 picogram lunar ejecta orbits associated with meteor streams were initiated, and the first results have been reported [5]. The earlier investigations did not find any significant number of long lifetime orbits, and the recent calculations substantiates the previous work. Thus, lunar ejecta are not expected to be responsible for a permanent enhancement of picogram dust particle flux in the vicinity of the earth from sporadic or normal shower meteoroid bombardment of the lunar surface. This does not rule out the possibility of a catastrophic large crater-forming event dumping a hugh quantity of dust into cislunar space with a significant quantity remainign for many years. However, the particles below 10 micron in diameter will still eventually leave the earth -moon system, largely in an anti-solar direction.

The current calculations have concentrated on studying the nature of the orbits of ejecta related to primary shower meteoroids.

For a given shower occurrence, the initial boundary conditions are determined. The ejecta particles having sufficient velocity to escape the moon will leave the surface with angles between 75° and 90° with respect to the shower particle radiant [8]. This angle has been designated Φ, while the position angle of the moon with respect to the earth during a shower period is θ (the angles are with respect to a coordinate system based on 0° being in the anti-solar direction). For the 5 picogram particles, the characteristics of the orbits in cislunar space is very dependent on the shower radiant and the angle θ. The previous report [3] giving the initial results of these calculations on Geminid related particles, showed that there were initial positions where

(1) no particles came near the earth or stayed in the earth-moon system for any length of time,

(2) particles streamed by the earth, but left the systme in a very short time,

(3) particles went into orbits of many months with several passes near the earth before leaving the system, and

(4) particles impacted the earth or the moon.

The largest number of orbits fell in (1) and (2) catagories. The (3) catagory particles are of special interest because they represent the only group with any real chance of detection near the earth. Consequently, surveys of the possible lunar ejecta orbits during the Geminids and Perseids showers through 1971 have been studied.

Figures 3 and 4 show examples of lunar ejecta orbits as the two parameters θ and Φ are varied during a 1969 Perseid shower period. With θ of 176°, and Φ varying between 25° and 40°, it is readily seen

that the orbits are scattered throughout three quadrants and they all leave in an anti-solar direction because of radiation pressure. In the next set of orbits, θ has changed to 179°, and with Φ varying between 25° and 32°, the particle orbits bend closer to the earth with Φ = 25° being quite close to the earth.

In fig. 4, the orbit for θ = 184°, Φ = 32° shows a moderately long lifetime orbit with several near-earth passes. The second set of orbits in fig. 4 shows variations obtained as θ moves through the positions where the particles pass near the earth and then scatter throughout all quadrants (Φ held constant at 25°). As Φ moves from 182° through 184° and above, the particles exhibited tight orbits around the earth before scattering. When a favorable θ - Φ combination coincides with the peak day of a shower, some of the lunar ejecta material may exist in the vicinity of the earth for significant periods of time. However, the particles would be in the 5 picogram mass range and would not have lifetimes of several decades. These longer lifetimes are necessary for a significant enhancement of the dust particle flux near the earth.

5. CUMULATIVE FLUX MODELS AND LUNAR EXPLORER 35 DATA

5.1 CUMULATIVE FLUX MODEL -- MCDONNELL [11].

McDonnell has presented an objective and comprehensive compilation and evaluation of a major portion of the data from the many dust particle experiments launched on rockets, satellites, and space probes [11]. A cumulative flux model was derived for (1) momentum detecting devices, and (2) penetrating sensors near the earth. A thorough discussion was given concerning the reliability of the data, particularly

that from single sensor microphones, especially where the experiment derived fluxes for similar portions of a cumulative flux curve were found to vary as much as three orders of magnitude. Establishing confidence in a single sensor data point was difficult. However, when several data points were analyzed and correlation established between several points, the confidence level in these data increased. This became even more evident when some of the data points were from later experiments which included coincidence sensors in the detector array. McDonnell used this approach in arriving at his cumulative flux-mass distribution curve derived from the acoustical sensor data [11].

5.2 GENERAL COMMENTS ON RELIABILITY OF DATA. As far back as the OSU rockets, the thermal environment of acoustical detectors was recognized as being critical. The problem was proved to be very complex and has never been completely solved. However, testing in laboratories and correlation studies of the in-flight thermal and experiment data did not show conclusively that in-flight experimental events were related to the thermal environment of the dust particle sensors and/or experiment instrumentation (Bohn, et al: [12]). Berg [13] recently reported data from Pioneer 8 and 9 which showed noise pulses from the microphone sensor during large solar proton events. There was a large solar flare event detected on both Mariner II and Mariner IV [14,15]. The acoustical detector registered no events in either case. Solar flare data have been obtained for the ten year period starting with September 1959 (Vanguard III). To date, for the spacecraft whose data are readily available, no correlation between solar flare events and microphone data have been seen. Data

from energetic proton experiments from all spacecraft since Explorer I are being compiled. When this effort is completed, a more definitive statement can be make concerning noise derived from energetic protons in the dust particle data since 1958.

It is not possible to eliminate all noise problems. Control and coincidence sensors greatly increase the reliability of the data. When data from the early years correlates with later data, the confidence level in the early data should increase.

5.3 SUMMARY OF SELECTIVE LUNAR, CISLUNAR AND INTERPLANETARY DATA. Alexander, et al [4], and McDonnell [11] have pointed out that over the entire range of in situ dust particle measurements, there is good agreement between the selenocentric, cislunar, and interplanetary space data, while the data from experiments near the earth show very poor agreement. In this paper, data are analyzed from all experiments (excluding near earth experiments) for which the authors are familiar with experiment performance including pre-and post-launch operation. This does not exclude other experiments in the same regimes of space, for all data is contained in the McDonnell [11] curve. The data in this paper will be compared to the above model. The experiments used are Mariner II, and IV, and Pioneer 8 and 9 in interplanetary space; Lunar Explorer 35 and Lunar Orbiter in selenocentric space; and OGO III and Pioneer I in cislunar space. The OGO III data point is that one recently reported as changed [5] due to a reexamination of the realtime and playback data from OGO III.

5.4 CUMULATIVE FLUX-MASS DISTRIBUTION CURVE FOR MASSES LESS THAN 10^{-9} gms. Data from the experiments listed above were fitted to a linear curve by applying linear regression curve fitting techniques.

Using the empirical equation $\Phi = km^{-a}$, where Φ is the flux [$p(m^2 \text{ sec } 2\pi \text{ sr})^{-1}$], m is the mass (gm) and k and a are constants, the lon equation [$\log \Phi = \log k - a \log m$] is linear with a slope of -a. The best curve fit gives a = 0.83. This curve is shown in fig. 5. An additional comparison of the data can be done by normalizing all experiment data points, using a = 0.83, to $m = 10^{-11}$ gm for comparison. The Φ for the derived curve at $m = 10^{-11}$ gm is 1.15×10^{-4} p $(m^2 \text{ sec } 2\pi \text{ sr})^{-1}$. The extreme Φ's are those of Lunar Explorer 35 coincidence data point (lowest) and Pioneer I (highest). These are less than an order of magnitude apart.

Normalized data: Φ in $p(m^2 \text{ sec } 2\pi \text{ sr})^{-1} \times 10^{-4}$	Spacecraft Exp.
3.0	Pioneer I
2.0	Pioneer 8 & 9
1.1	Mariner IV
0.78	Lunar Explr. 35 (mic)
0.77	OGO III (film)
0.91	Lunar Orbiter
0.5	Lunar Explr. 35 (coinc. cap-mic)

The other information shown in fig. 5 consists of the two cumulative flux-mass distribution curves derived from zodiacal light models and recently reported by Giese [16]. The slope of the curve derived from the several experiments is in the direction of The Type II (k = 2.5) curve. All of the data lies between the two curves.

5.5 COMPARISON OF THE SELECTIVE DATA FLUX CURVE, THE McDONNELL MODEL, AND SUMMARY. The summary curves derived by McDonnell [11] are shown in fig. 6 along with the composite curve of fig. 5,

Giese's two zodiacal light flux curves, and the radar data to 10^{-6} gm of Nilsson and Southworth[17]. The a of the fig. 5 curve is less than McDonnell's curve, but the consistancy of the consistancy of the data is quite apparent.

The data in selenocentric space have been very consistent for almost four years. The periods when there are no major meteor showers give a flux that is in excellent agreement with that in cislunar and interplanetary space. There is no evidence of concentration or focusing. The fluctuations of the flux during major meteor showers has occurred over a four year period for the 5 picogram sensor, while the 100 picogram sensor has not shown such a correlation. The data used in fig. 5 are from experiments which first produced data in 1960 - 1962. These data are found to correlate extremely well with the data from the still active experiments: Lunar Explorer 35 and Pioneer 8 & 9. The consistancy of the data over a period of a decade indicated that the initial measurements were basically reliable and a true indicator of the data to come.

6. ACKNOWLEDGEMENT

The work was partially supported under NASA Research Grant NGR 39 - 012 - 001.

7. REFERENCES

[1] T. N. Nazarova, Space Science Reviews, 8, p.455-466 (1968).

[2] C. A. Gurtler and G. W. Grew, Science, 161, 462 (1968).

[3] W. M. Alexander, C. W. Arthur, J. D. Corbin, and J. Lloyd Bohn, XIIth COSPAR Meeting, Prague (1969), Space Research X (North-Holland, Amsterdam, 1970) p. 252.

[4] W. M. Alexander, C. W. Arthus, and J. Lloyd Bohn, XIIIth COSPAR Meeting, Leningrad (1970), Space Research XI (Akademie-Verlag, Berlin 1971) p. 279.

[5] W. M. Alexander, C. W. Arthur, J. Lloyd Bohn, J. H. Johnson, and B. J. Farmer, XIVth COSPAR Meeting, Seattle (1971), Space Research XII (Akademie-Verlag, Berlin, 1972) in print.

[6] C. S. Nilsson, Aust. J. Phys., 1964, 17, p 205.

[7] C. A. Gurtler and G. W. Grew, Science, 161, 426 (1968).

[8] D. Gault, private communication.

[9] C. W. McCracken, NASA SP-135 p. 213-224 (1965).

[10] I. I. Shapiro, D. A. Lautman, G. Colombo, J. Geophys Res. 71, 5695 (1966).

[11] J. A. M. McDonnell, XIIIth COSPAR Meeting, Leningrad (1970).

[12] J. Lloyd Bohn, W. M. Alexander, and W. F. Simmons, Xth COSPAR Meeting, London (1967), Space Research VIII (North-Holland, Amsterdam, 1968) p. 588.

[13] O. E. Berg, U. Gerloff, XIIIth COSPAR Meeting, Leningrad, 1970, Space Research XI (Akademie-Verlag, Berlin, 1971.

[14] H. R. Anderson, Science, 138, 3545 (1962).

References Cont'd:

[15] H. R. Anderson, Science, 149, 1240 (1965).

[16] R. H. Giese, XIVth COSPAR Meeting, Seattle, 1971 (Akademie-Verlag, Berlin, 1972).

[17] C. S. Nilsson and R. B. Southworth, Physics and Dynamics of Meteors (D. Reidel Publ. Co., Dordrecht, Holland, 1968) p. 280-327.

8. FIGURE CAPTIONS

FIGURE 1: Histogram of 5 picogram particle event rates: D201-1967 to D365-1970.

FIGURE 2: Event rates for six major meteor showers over four years: 1967 - 1970.

FIGURE 3: Shower related lunar ejecta orbits I.

FIGURE 4: Shower related lunar ejecta orbits II.

FIGURE 5: Log cumulative flux-mass distribution for masses less than 10^{-9} gms.

FIGURE 6: Comparison of fig. 5 log cumulative flux-mass distribution curve with the McDonnell Models

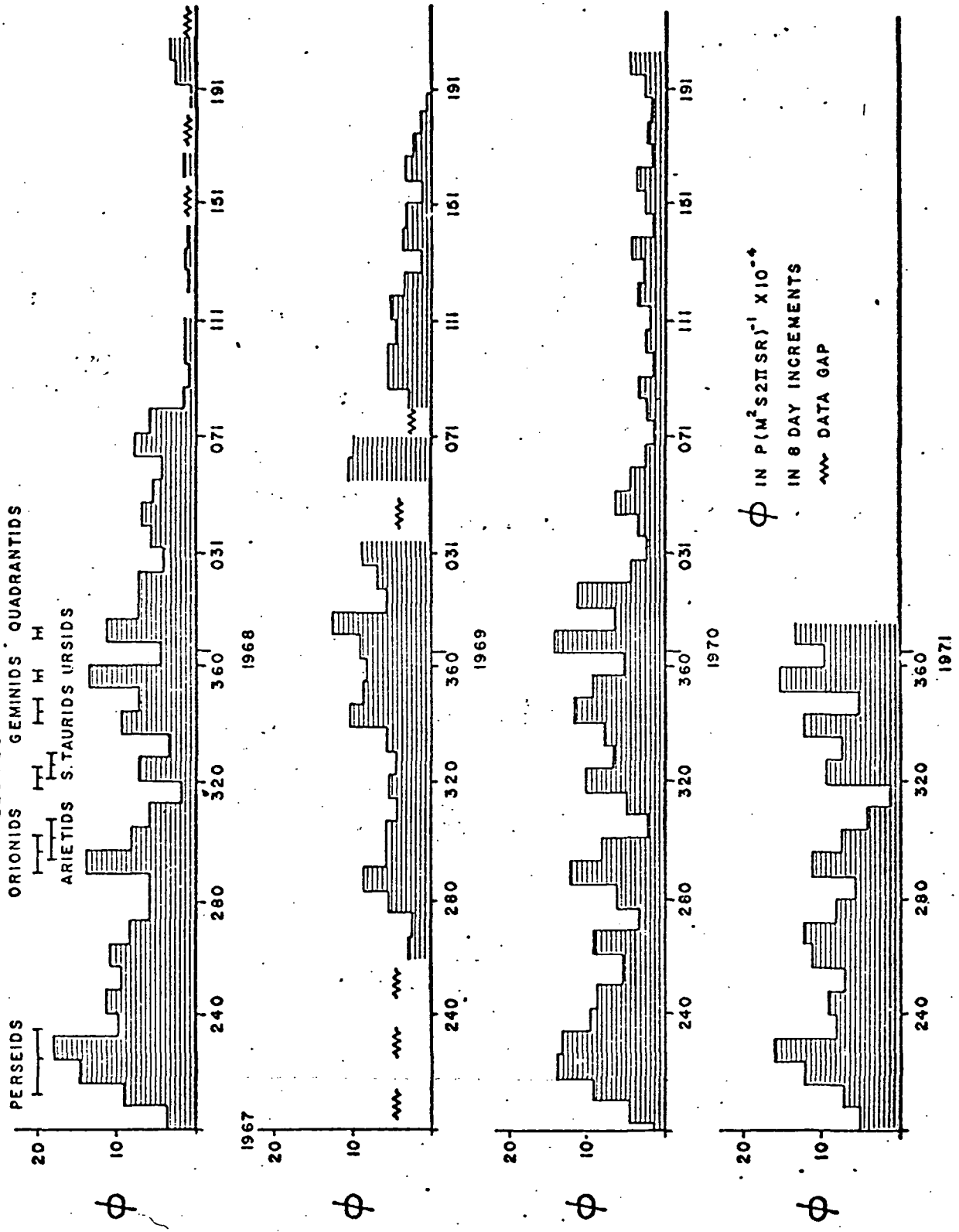
PERSEIDS
ORIONIDS
LEONIDS
ARIETIDS
GEMINIDS
S.TAURIDS
QUADRANTIDS
URSIDS
1967
1968
1969
1970
1971
φ IN P(M²S2πSR)⁻¹ X10⁻⁴
IN 8 DAY INCREMENTS
DATA GAP

FIGURE 1

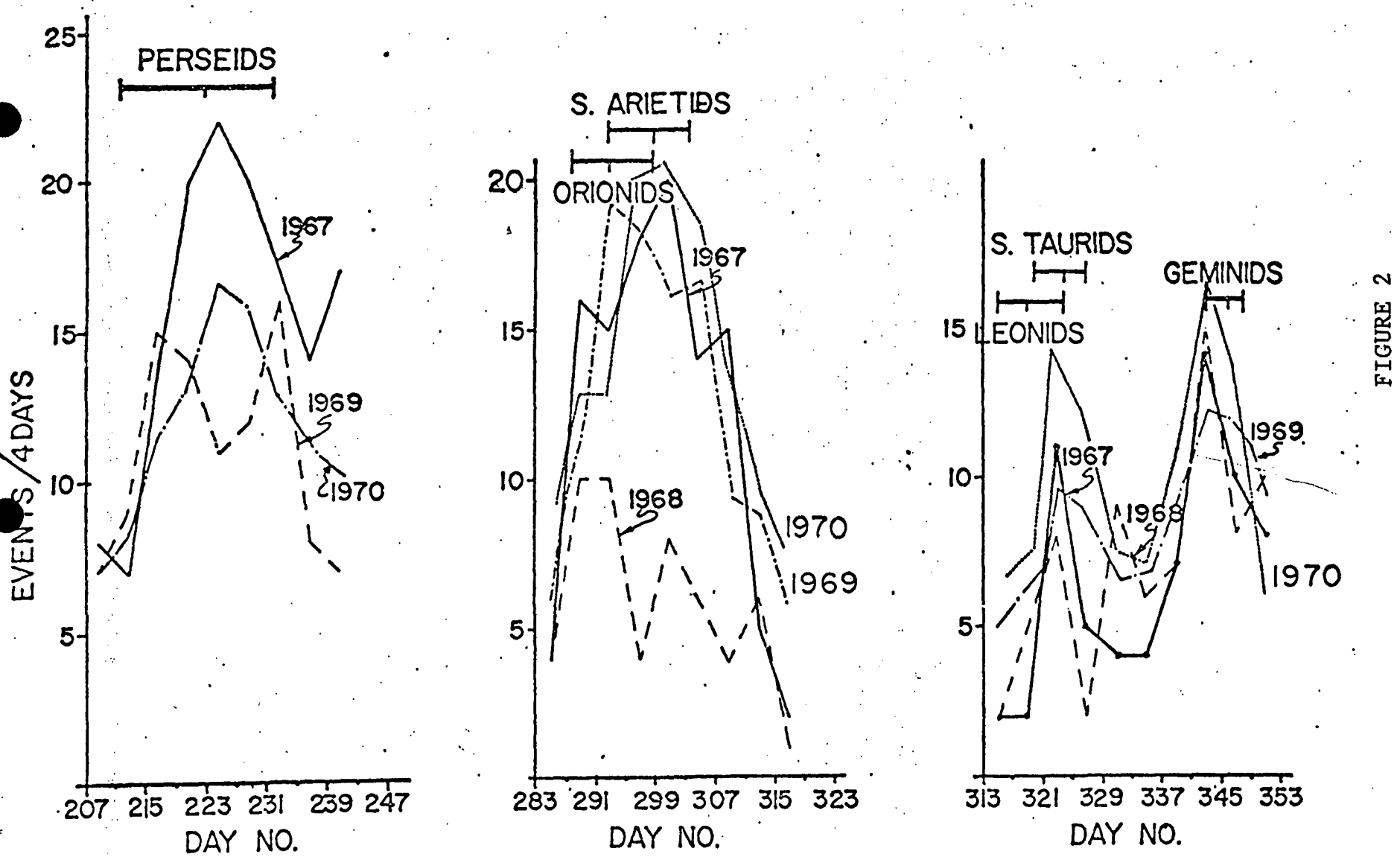
PERSEIDS
S. ARIETIDS
ORIONIDS
S. TAURIDS
LEONIDS
GEMINIDS
1967
1968
1969
1970
EVENTS/4DAYS
DAY NO.
DAY NO.
DAY NO.
25
20
15
10
5
207 215 223 231 239 247
283 291 299 307 315 323
313 321 329 337 345 353

FIGURE 2

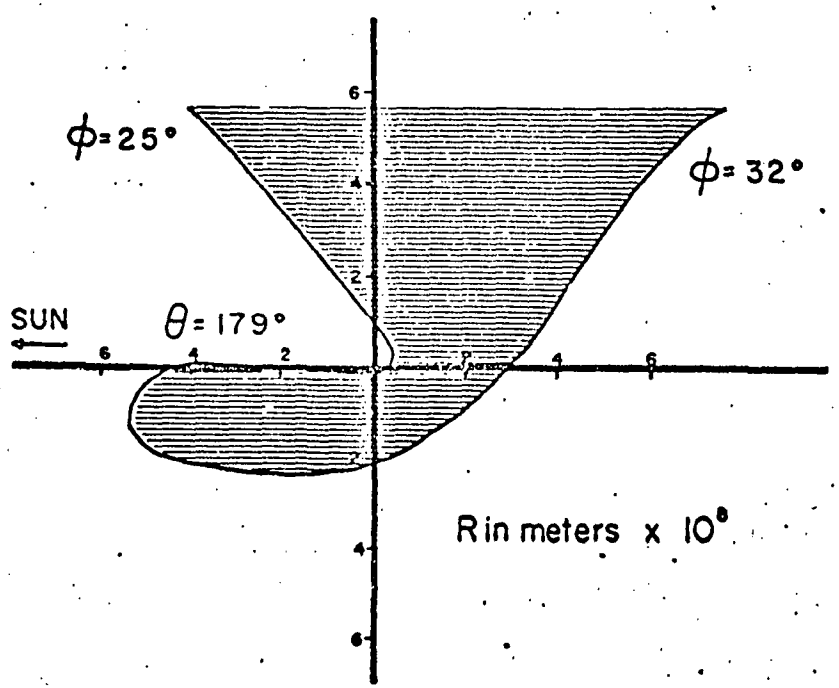
ϕ=25°
ϕ=32°
SUN
θ=179°
6
4
2
2
4
6
R in meters x 10⁸

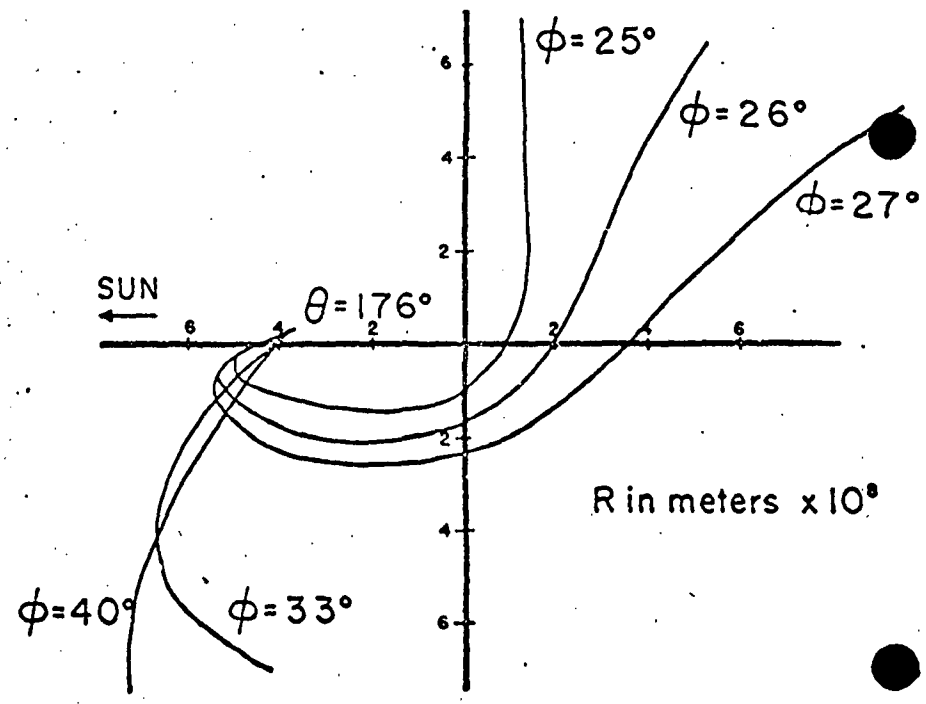
ϕ=25°
ϕ=26°
ϕ=27°
SUN
θ=176°
6
4
2
2
4
6
R in meters x 10⁸
ϕ=40°
ϕ=33°

FIGURE 3

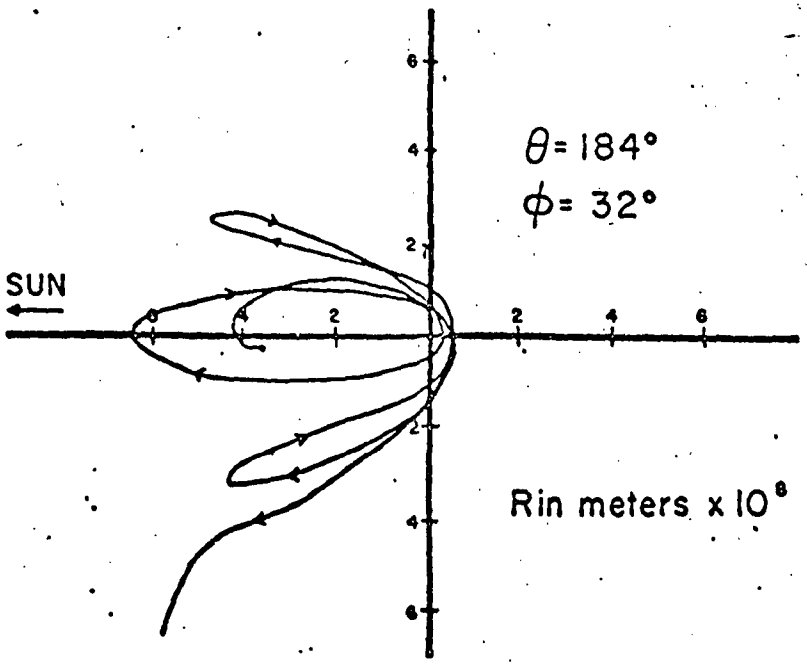
θ = 184°
ϕ = 32°
SUN
Rin meters x 10⁸

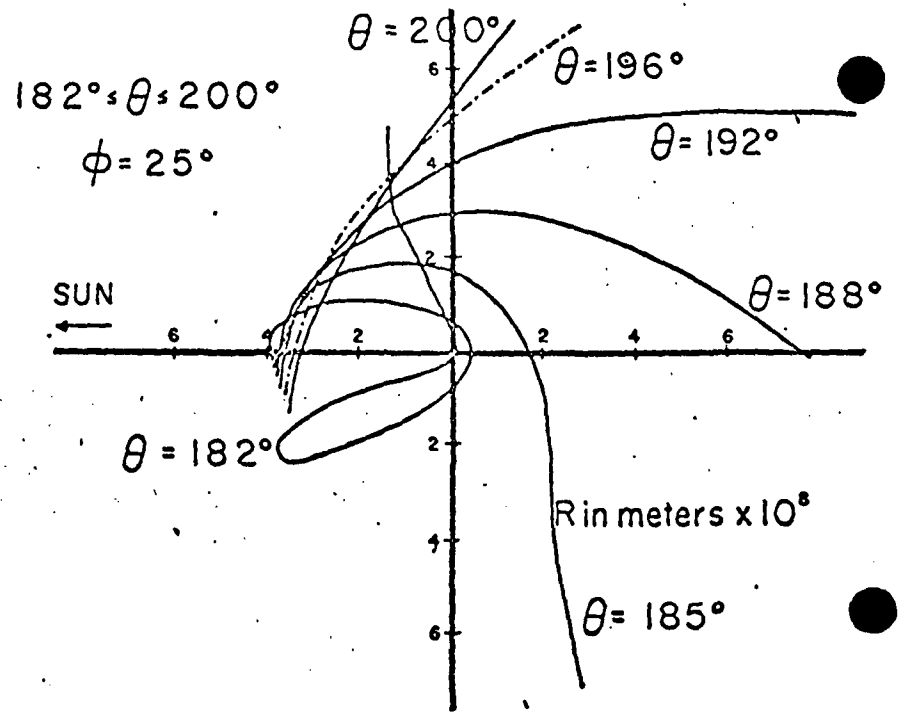
182° ≤ θ ≤ 200°
ϕ = 25°
θ = 200°
θ = 196°
θ = 192°
θ = 188°
θ = 182°
θ = 185°
SUN
Rin meters x 10⁸

FIGURE 4

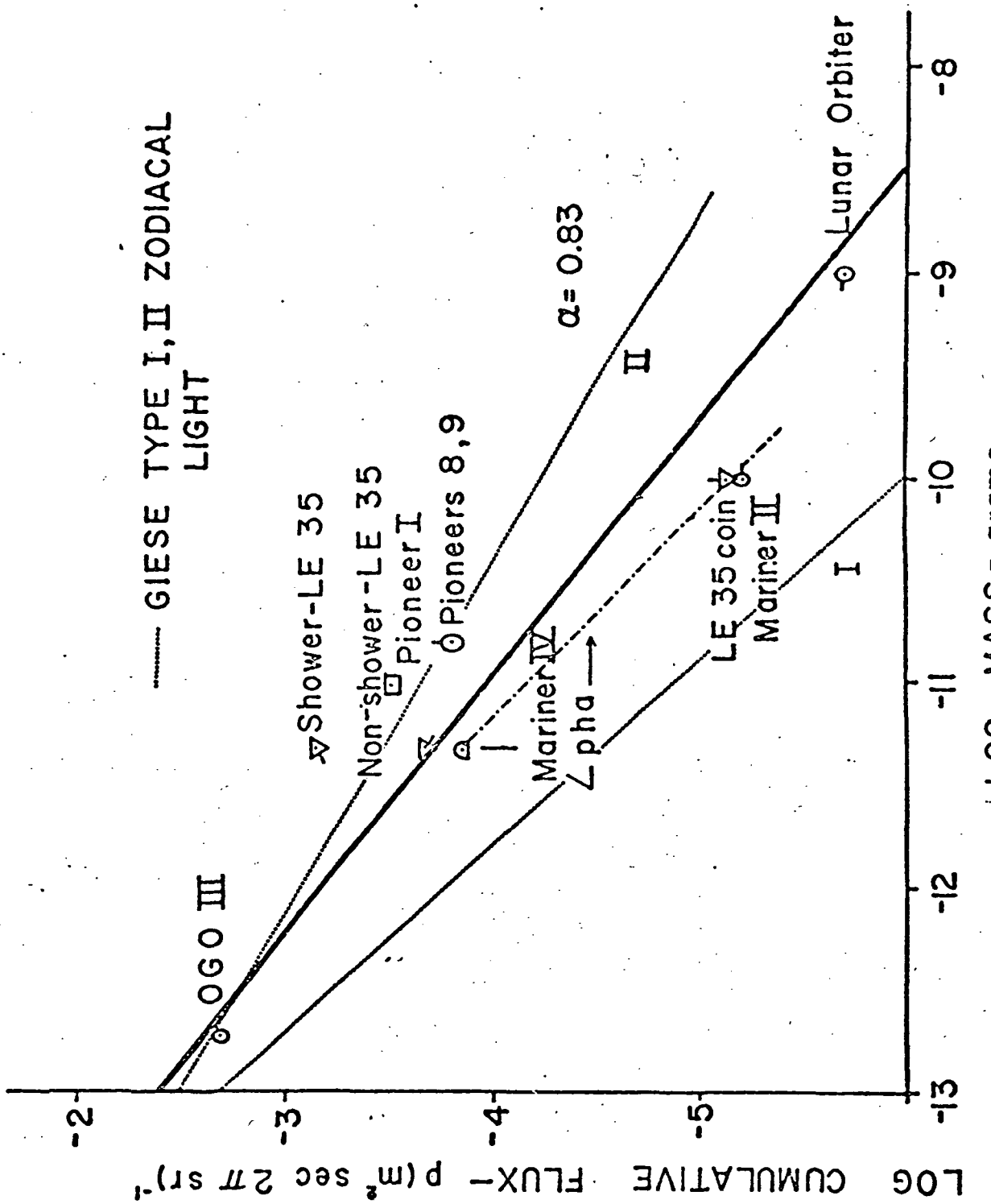
LOG CUMULATIVE FLUX- p(m² sec 2π sr)⁻¹
-2
-3
-4
-5
LOG MASS - grams
-8
-9
-10
-11
-12
-13
Lunar Orbiter
α= 0.83
II
I
III
OGO III
Shower-LE 35
Non-shower-LE 35
Pioneer I
Pioneers 8,9
Mariner IV
pha
LE 35 coin
Mariner II
GIESE TYPE I, II ZODIACAL LIGHT

FIGURE 5

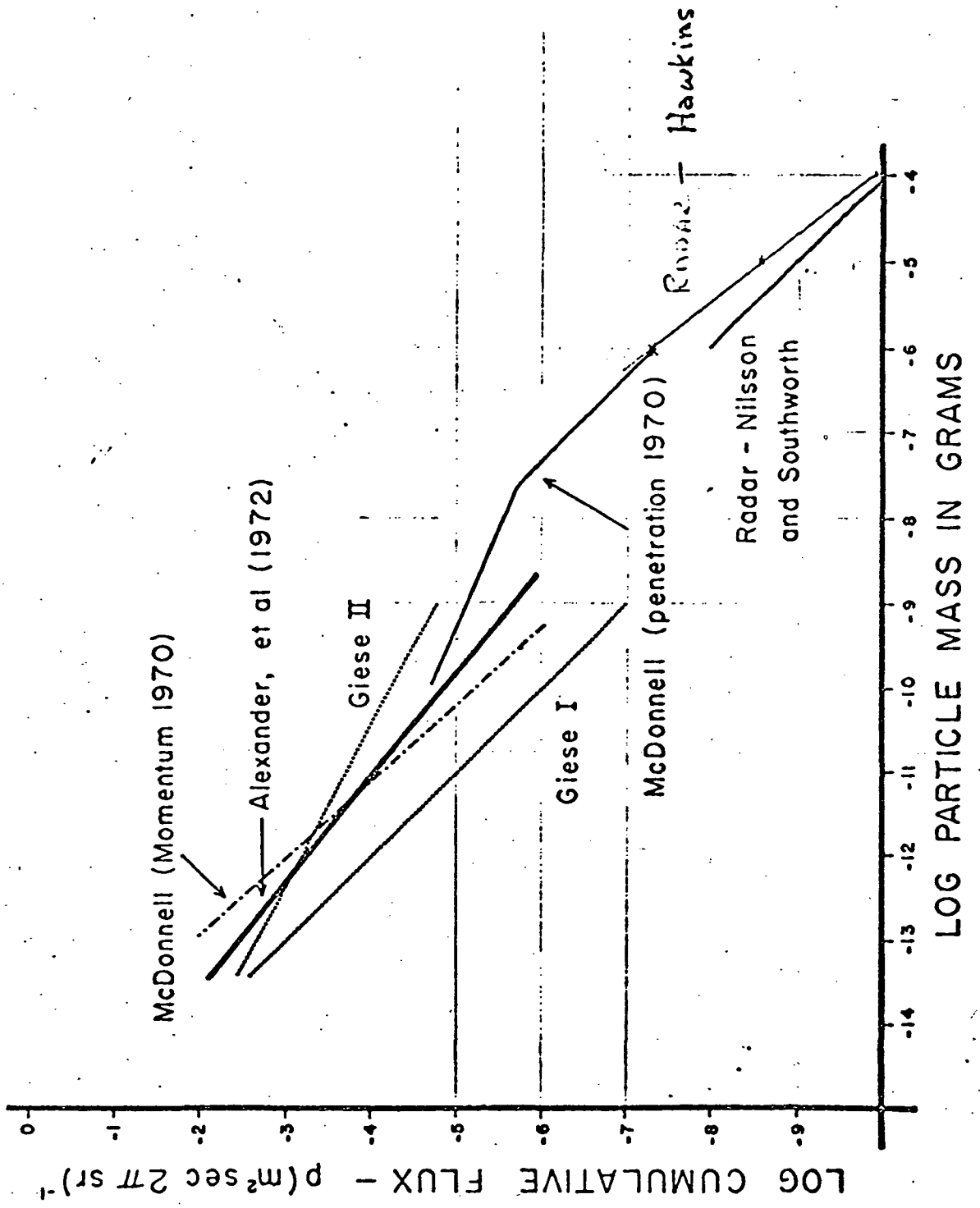
LOG CUMULATIVE FLUX – p(m²sec 2π sr)⁻¹
LOG PARTICLE MASS IN GRAMS
McDonnell (Momentum 1970)
Alexander, et al (1972)
Giese II
Giese I
McDonnell (penetration 1970)
Radar - Nilsson and Southworth
Hawkins

FIGURE 6

III. Additional Analysis of Mariner IV Data

A. The launch and mission of Pioneer 10 represented the second U. S. A. spacecraft which transversed heliocentric space past 1.1 AU. An additional look at the Mariner IV (M IV) measurement was accomplished. The major portions of the M IV data not previously reported was given in a paper prepared for the XVIth meeting of COSPAR. The paper is given in section III B.

At the XVI COSPAR meeting a paper by McDonnell (1) was presented containing data from Pioneer 8 and 9 which allowed a determination of the cumulative flux-mass distribution over a mass range of 0.1 picograms to 10 picograms. The M IV measurement provides a determination of this flux from 10 picograms to 1 nanogram. Figure III-1 shows an overall cumulative flux-mass distribution containing the pertinent data from in-situ measurements, lunar microcrater studies, zodiacal light, radar and visual. The combined Poineer 8-9 and M IV provides a very consistant cumulative flux determination for 4 orders of magnitude and only two measurements.

FIGURE III-1 REFERENCES

(1) McDonnell, J. A. M.; Space Research XIV (1974), in press

(2) Alexander, W. M., J. L. Bohn; Space Research XIV, (1974), in press

(3) Schneider, E., D. Storzer, A. Mehl, J. B. Hartung, H. Fechtig, W. Gentner; Proc. Fourth Lunar Sci. Conf., Pergamon Press (1973), in press

(4) Giese, R. H.; Space Research XII, 437 (1972)

(5) Neukum, G., F. Horz, J. B. Hartung, D. A. Morrison; Proc. Fourth Lunar Sci. Conf., Pergamon Press (1973), in press

(6) Hartung, J. B., F. Horz, K. F. Aitken, D. E. Gault, D. E. Brownlee; Proc. Fourth Lunar Sci. Conf., Pergamon Press (1973), in press

(7) Hughes, D. W.; Planet. and Space Sci., (1974), in press

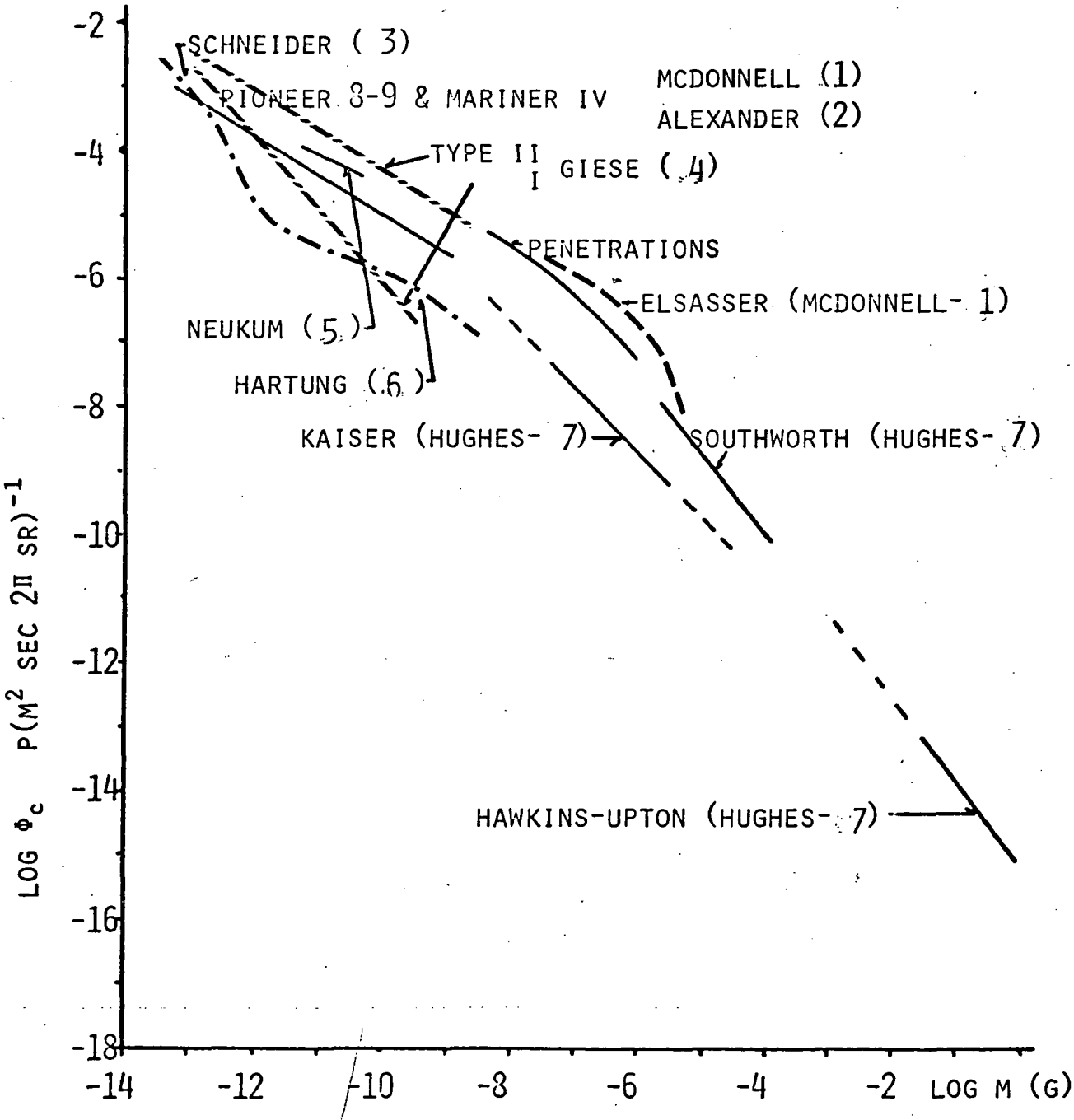

FIG. III-1: OVERALL CUMULATIVE FLUX-MASS DISTRIBUTION

(Summary paper presented at XVI th COSPAR and submitted to Space Research XIV)

MARINER IV: A STUDY OF THE CUMULATIVE FLUX OF DUST PARTICLES OVER A HELIOCENTRIC RANGE OF 1 TO 1.56 AU 1964 TO 1967

W.M. Alexander (Max-Planck-Institut für Kernphysik, Heidelberg, FRG) and
J. Lloyd Bohn (Temple University, Philadelphia, Pennsylvania, USA).

ABSTRACT:

Between December 1964 and December 1967, the Mariner IV dust particle experiment obtained data concerning the distribution of minute Zodiacal Dust Cloud particles over a heliocentric range of 1 to 1.56 AU. The first measurement was over the complete heliocentric range, while the two additional measurements were made between 1.1 and 1.25 AU in 1966, and 1.2 to 1.5 AU in 1967. The initial results of these measurements presented the mean cumulative flux for the respective data periods. The results of a detailed study and comparison of the three measurements are presented, with particular emphasis on the variation of the flux as a function of heliocentric range. A small, but statistically significant, increase in the flux is observed between 1.15 and 1.4 AU. The initial reports showed a lower cumulative flux for the latter two measurements. However, a detailed analysis containing corrections for spacecraft attitude indicate that all three measurements yield similar results, and that the particles detected were in low inclination orbits.

1. INTRODUCTION

The Mariner IV Spacecraft was launched on 30 November 1964 and reached a near encounter with Mars on 15 July 1965. The cosmic dust experiment detected interplanetary dust particles impacting an exposed sensor plate. Except for the time used for playback of data from the photographic experiment immediately after the encounter, data of the cosmic dust experiment was continuous from launch until 1 October 1965 when the earth-spacecraft distance became too great for successful data transmission. In 1966 and 1967 signals from the spacecraft were reacquired and information received from the dust experiment. The mean cumulative flux for the heliocentric range of the experiment over the times of data reception have been reported. The purpose of this paper is to [1] give a summary of the statistical analysis of the data, [2] present the events as a function of heliocentric range, and [3] show the cumulative flux-mass distribution as derived from the Mariner IV measurements.

2. MARINER IV COSMIC DUST EXPERIMENT

A description of the experiment was originally reported by Alexander et al (1). Further studies concerning calibration of piezoelectric acoustical transducers bonded to large impact plates by McDonnell (2) provided a shift in the threshold impulse of the Mariner IV experiment. This was first reported by McDonnell (3) as a mass threshold of 6×10^{-12} g or an impulse of 1.2×10^{-5} dyne-sec for 20 km/s^{-1} particles, which was lower than first reported (1). The number of events has remained the same since the first report.

3. NOISE AND MARINER IV

Noise has been an ever present problem with all of the very low data rate dust particle experiments. Several papers have presented data concerning noise from the standpoint of thermal problems and solar energetic particles (4,5,6,7). From the extensive tests by Bohn et al (5), there appears to be little reason to suspect that the events in the data are caused by thermal related phenomena. The solar energetic particle events during the mission are shown with the data in fig. 1. The Mariner IV instrument does not show any evidence of the kind of events reported from Pioneer 8 and 9 (6,7). One large event occurred during an eight day period of zero counts from the microphone sensor. There does not appear to be any compelling reason or evidence that the Mariner IV data is subject to noise interference.

4. DATA FROM THE MARINER IV EXPERIMENT

4.1. Event Information. The cosmic dust experiment detected 241 events during the primary phase of the mission. The data are shown in fig. 1 as events vs heliocentric ranges. A pulse height analysis (PHA) was made on each event. The PHA information was erased after each readout of the experiment information. However, a cumulative counter was never reset and provided a continuous count of the number of events if any short periods occurred where data was not received or processed. Of the 241 events, 23 occurred during periods where in-flight PHA information was not processed. Therefore, the total cumulative flux can be derived from the 241 events, and the slope of the cumulative flux-mass distribution from the remaining 218 events.

4.2. Experiment Attitude Information. The attitude of the experiment was such that the normal of the impact plate was in or very close to the ecliptic plane. Also, an angle of 90° with the radius vector to the sun was maintained throughout the mission.

4.3. Summary of Statistical Evaluation of the Data. The distribution of the events in time were considered to be represented by a Poisson distribution, and the Chi squared test for variance was employed to test the degree of randomness of the event time intervals. First, all 241 events were used. χ^2 was found to be 22 (5 degrees of freedom) giving a probability of less than 0.001 that the overall distribution was randomly distributed in time. However, when the distribution is considered in three segments, near earth, near Mars, and between the orbits of the two planets, the following values for p were found: [1] earth to 1.2 AU, p=0.7 [2] 1.2 to 1.45 AU. p=0.6; and [3] 1.45 to 1.56 AU, p=0.95. The events within each segment are definitely distributed in time in a random manner.

5. DISCUSSION OF THE MARINER IV RESULTS

5.1. Flux vs Heliocentric Range. The data seen in fig. 1 shows an increase in flux between the planets. A search was conducted for possible interceptions of nodes of cometary orbits or meteor streams as possible sources of flux increase between the planets. However, only one was found near the Mariner IV orbit and the increase is much too broad for a single stream. Intercepts of the planes of cometary orbits with the ecliptic plane along the Mariner IV path were studied. It has been shown in a number of studies (8,9,10,11) that the semi-major axis of orbits of small particles, after being created by any process, will be considerably larger (i.e., those not moving into parabolic or hyperbolic orbits). It is not clear

that such an increase as seen by Mariner IV can occur for this reason. A test of this occurred when spacecraft transmission was reacquired in 1966. The spacecraft was near perihelion, and then started out again. The mean flux value was essentially the same as for the first part of the mission, and then increased with heliocentric range. However, the solar ecliptic longitude was quite different. Therefore, the probability of a significant increase in one segment of solar ecliptic longitude due to debris from cometary orbits is felt to be low.

The mean flux values derived from the periods in 1966 and 1967 were modulated by shifts in the spacecraft attitude. The normal to the detector plate was as previously stated when the canopus sensor was locked on Canopus. About 1 September 1966 the Canopus sensor was found to be locked on a star near the ecliptic plane. The plane of the detector plate was then lying in the ecliptic plane with the plate normal pointing to a pole in the celestial hemisphere. The flux was found to be significantly reduced - the ratio of the rates was a factor of four. This is strong evidence that the orbit inclination angles of the detected particles are quite low. Significant flux range data is found in Table 1.

The measurement is considered to show depression in flux at the planetary orbits. The most probable cause being that of planetary scattering. This is not an effective mechanism for particles in these size regimes with fairly short lifetimes. However, the effect may be significant with particles of these sizes when inclinations and eccentricities are low in value (12).

5.2. Cumulative Flux-Mass Distribution. The PHA measurements provide a means for determining the cumulative flux-mass distribution for detected events. The data were fitted to a linear curve by applying linear regression curve fitting techniques. The cumulative flux is usually described by using the empirical equation $\Phi = km^{-\alpha}$, where Φ is flux in (particles m^{-2} s^{-1}) m is the mass (g) and k and α are constants.

The log equation: $\log_{10}\Phi = \log_{10} k - \alpha \log_{10} m$ is linear with slope of $-\alpha$. The values for α were found for each segment, and the variation fell within statistical bounds. The overall cumulative flux is presented in fig. 2 since the slope variation was not significant.

6. COMPARISON OF MARINER IV CUMULATIVE FLUX WITH OTHER IN-SITU MEASUREMENTS

6.1. Selected In-Situ Measurements. The measurements selected for comparison with Mariner IV results in fig. 3 were chosen because they contained either coincidence information or some form of control to enhance the reliability of the data. The data from the penetration experiments of Explorer's XVI and XXIII and Pegasus are used. The penetration points contain the calibration revisions which have occurred since the review paper of McDonnell (3).

6.2. Selected Ground-Based Data. The radar data from two representative sources are used (13, 14), for comparison of the particles just larger than those obtainable from the in-situ measurements.

6.3. Results of Comparison. The cumulative flux-mass distribution from the in-situ measurements has a slope essentially identical with that determined by the Mariner IV measurements. The Mariner IV slope used in fig. 3 is that between 1 and 1.2 AU. The decrease of the slope from radar through the Pegasus and Explorer points shows an agreement which is quite close. All points of the curve have been corrected for gravitational focusing (15, 16) so the flux is that of interplanetary space near 1 AU. The in-situ measurements are not, at the present time, showing a mass cutoff; i.e. slope going to zero on the cumulative flux-mass distribution curve. In addition, information from the studies of sub-micron craters on lunar rocks show the presence of particle sizes smaller than previously expected (17, 18).

7. ACKNOWLEDGMENT

The work was partially supported under NASA Research Grant NGR 39 - 012 - 001 and the Max-Planck-Institut für Kernphysik. The authors are indebted to Dr. H. Fechtig, Dr. H.-J. Hoffmann, and Dr. E. Grün of the Max-Planck-Institut für Kernphysik for many helpful discussions.

8. FIGURE CAPTIONS

Figure 1: Mariner IV Events as a function of heliocentric range.

Figure 2: Cumulative flux-mass distribution derived from the measurement of Mariner IV.

Figure 3: Comparison of Mariner IV cumulative flux distribution and in-situ measurements.

Table (ref. 28). Comparison of Flux from Mariner IV for 1964-65, and 1966 over the same Heliocentric Range.

Range (AU)	Flux (events m^{-2} $s^{-1}x10^{-5}$) 1964 - 1965	1966
1.1-1.08	8	9
1.08-1.12	5	8
1.12-1.19	9	7
1.19-1.22	10	9
1.22-1.25	13	13

8. REFERENCES

(1) W.M. Alexander, C.W. McCracken, and J. Lloyd Bohn, Science, 149, 1240 (1965).

(2) J.A. M. McDonnell, J. of Physics E, Series 2, Vol. 2, 1026 (1969).

(3) J.A.M. McDonnell, Space Research XI, 415 (1971).

(4) C.S. Nilsson, Science, 153, 1242 (1966).

(5) J. Lloyd Bohn, W.M. Alexander, and W.F. Simmons, Space Research VIII, 588 (1968).

(6) O.E. Berg und U. Gerloff, Space Research XI, 225 (1971).

(7) O.E. Berg and E. Grün, XV th COSPAR Meeting, Madrid (1972), to be published in Space Research XIII.

(8) F.L. Whipple, Astrophysical J., 121, 750 (1955).

(9) M. Harwit, J. of Geophysical Research, 68, 2171 (1963).

(10) E.C. Silverberg, Dissertation, University of Maryland, Dept. of Physics and Astronomy, Tech. Report, No. 70-066 (1970).

(11) J.S. Dohnany, Icarus, 17, 1 (1972).

(12) T. Schmidt, NASA SP-150, 333 (1967).

(13) T.R. Kaiser, Monthly Notices Royal Astronomical Society, 123, 265 (1961).

(14) C.S. Nilsson and R.B. Southworth, Physics and Dynamics of Meteors, 280 (1968).

(15) E.J. Öpik, Proceedings of Royal Irish Academy, 54 Section A, 165 April (1951).

(16) B.G. Cour-Palais, NASA SP-8013 (1969).

(17) G. Neukum, E. Schneider, A. Mehl, D. Storzerm G.A. Wagner, H. Fechtig, and M.R. Bloch, XVth COSPAR Meeting, Madrid (1972), to be published in Space Research XIII.

(18) J.B. Hartung, F. Hörz, D.E. Gault, Proceedings of the Third Lunar Sci. Conf., Geochim. Cosmochim. Acta Suppl. 3, Vol. 3, 2735 (1972).

(19) W.M. Alexander, C.W. Arthur, J. Lloyd Bohn, J.H. Johnson, and B.J. Farmer, Space Research XII, 349 (1972).

(20) O.E. Berg and E. Grün, XVth COSPAR Meeting, Madrid (1972), to be published in Space Research XIII.

(21) W.M. Alexander, C.W. Arthur, and J. Lloyd Bohn, Space Research XI, 279 (1971).

(22) B. Konstantinov, M. Bredov, E. Mazets, V. Panov, R. Aptekar, S. Golenazky, Y. Gurian and V. Ilinsky, Cosmic Research 6, 738 (1968).

(23) B. Konstantinov, M. Bredov, E. Mazets, V. Panov, R. Aptekar, S. Golenazky, Y. Gurian and V. Ilinsky, Cosmic Research 6, 911 (1969).

(24) T.N. Nazarova, XV th COSPAR Meeting, Madrid (1972), Preprint.

(25) W.M. Alexander, Science, 138, 1098 (1962).

(26) W.M. Alexander, C.W. McCracken, and J. Lloyd Bohn, Science 149, 1240 (1965).

(27) D.E. Gault, Proceedings of the Third Lunar Sci. Conf., Geochim. Cosmochim. Acta Suppl. 3, Vol. 3, 2713 (1972).

(28) W.M. Alexander, C.W. Arthur, J.D. Corbin, and J. Lloyd Bohn, Space Research X, 252 (1970).

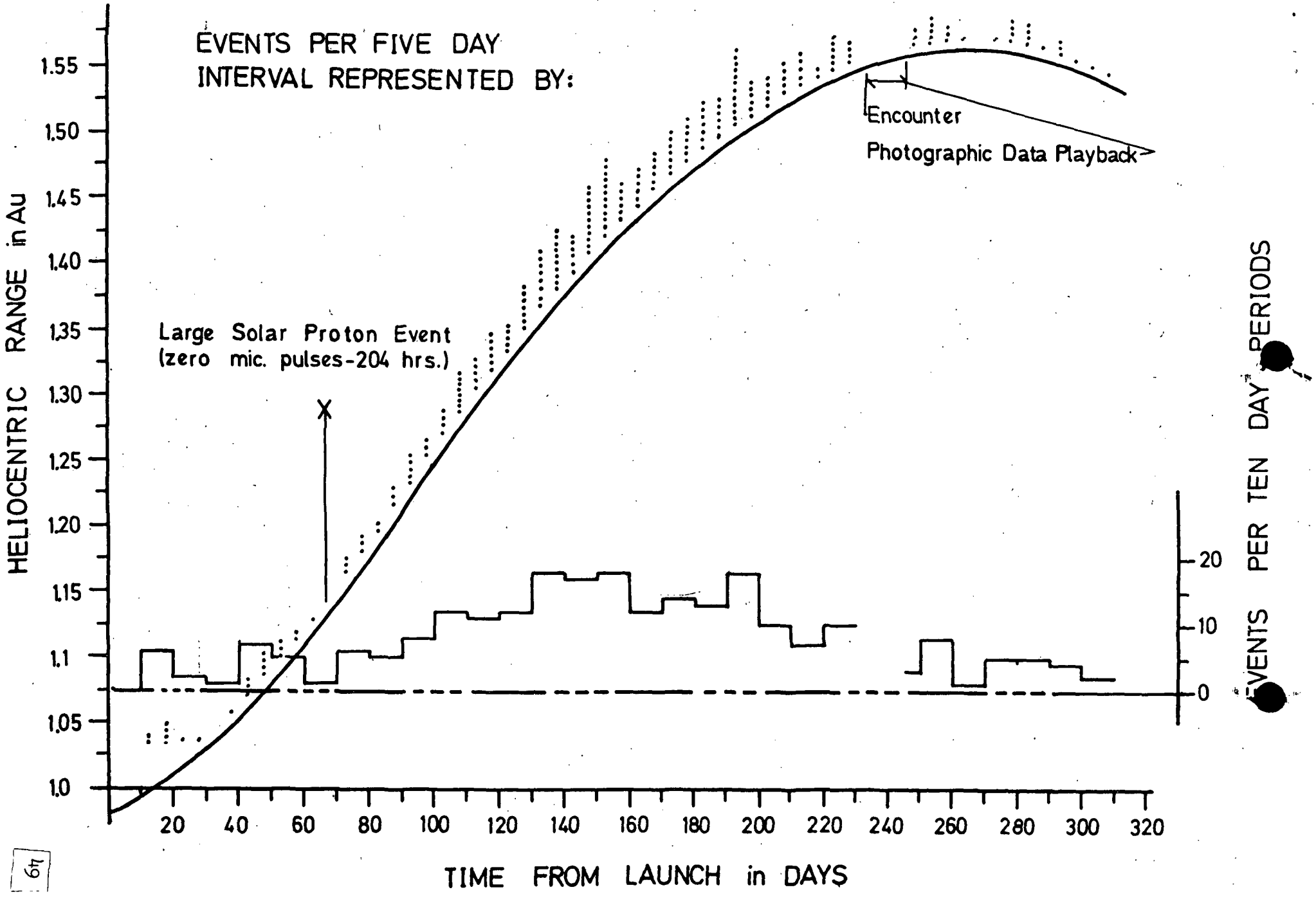
EVENTS PER FIVE DAY
INTERVAL REPRESENTED BY:
Encounter
Photographic Data Playback
Large Solar Proton Event
(zero mic. pulses-204 hrs.)
HELIOCENTRIC RANGE in Au
1.55
1.50
1.45
1.40
1.35
1.30
1.25
1.20
1.15
1.1
1.05
1.0
20
40
60
80
100
120
140
160
180
200
220
240
260
280
300
320
TIME FROM LAUNCH in DAYS
EVENTS PER TEN DAY PERIODS
20
10
0

Fig. 1

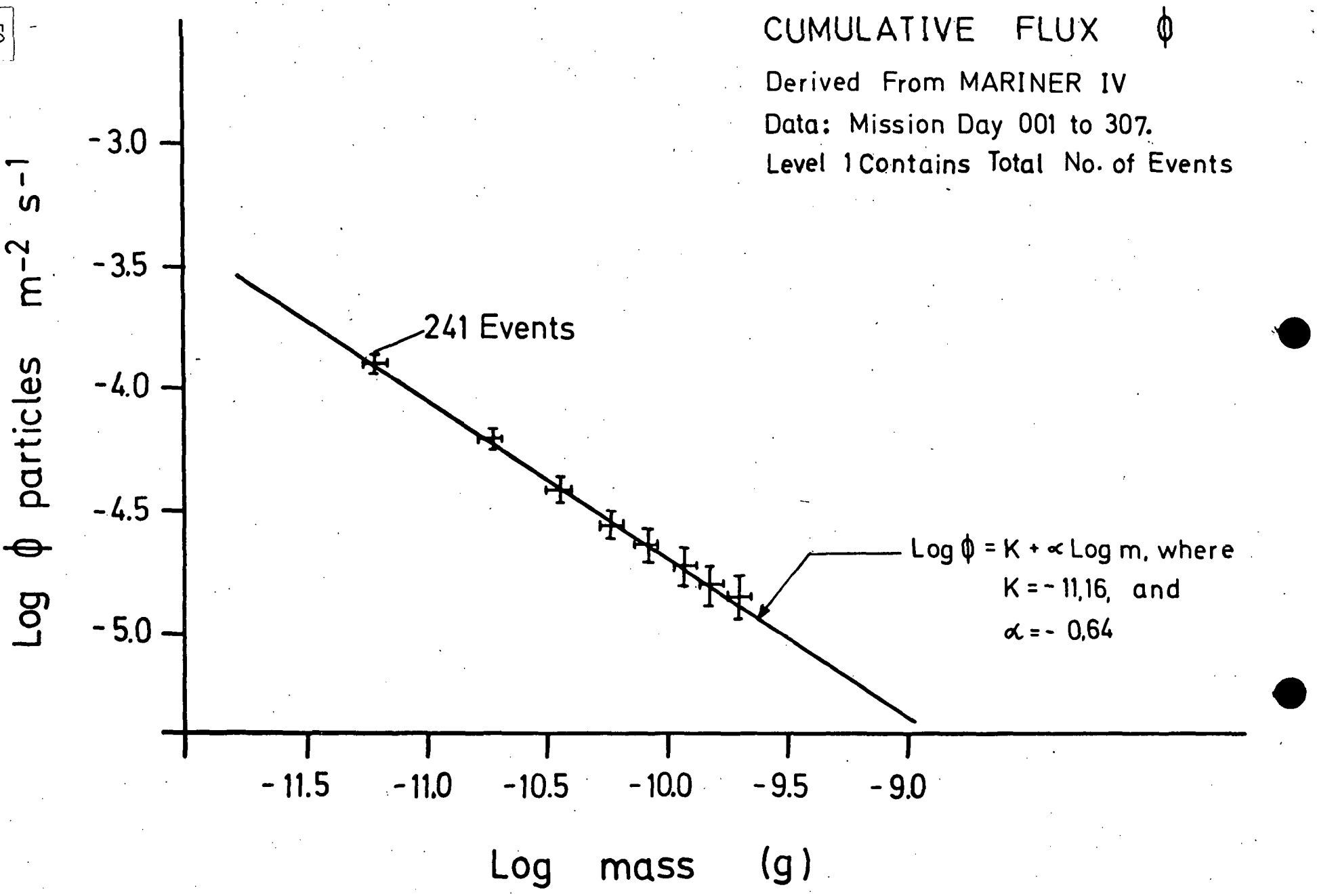
CUMULATIVE FLUX ϕ
Derived From MARINER IV
Data: Mission Day 001 to 307.
Level 1 Contains Total No. of Events
241 Events
Log ϕ = K + ∝ Log m, where
K = - 11,16, and
∝ = - 0,64
Log ϕ particles m⁻² s⁻¹
-3.0
-3.5
-4.0
-4.5
-5.0
-11.5
-11.0
-10.5
-10.0
-9.5
-9.0
Log mass (g)

Fig. 2

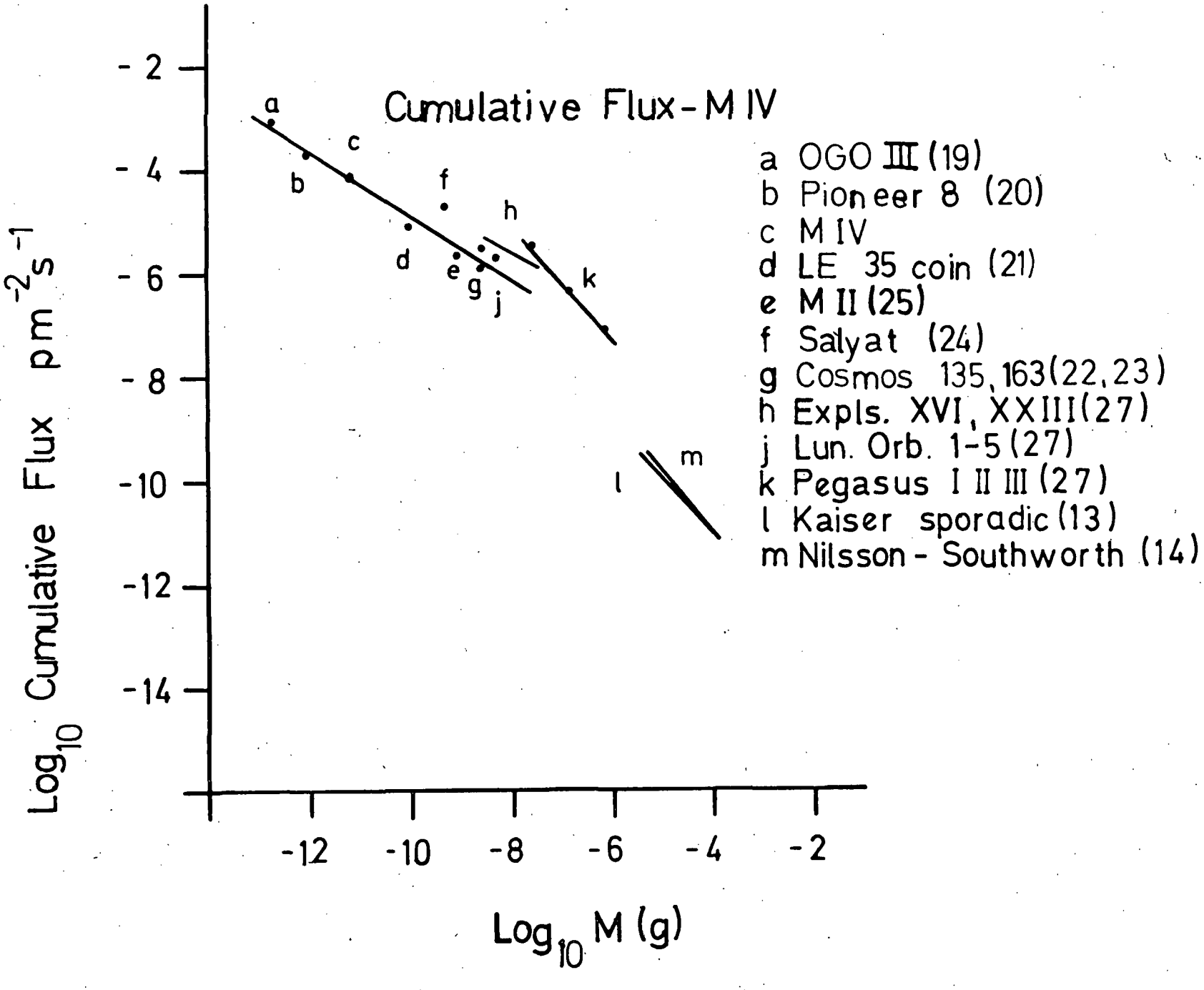
Cumulative Flux - M IV
a OGO III (19)
b Pioneer 8 (20)
c M IV
d LE 35 coin (21)
e M II (25)
f Salyat (24)
g Cosmos 135, 163 (22, 23)
h Expls. XVI, XXIII (27)
j Lun. Orb. 1-5 (27)
k Pegasus I II III (27)
l Kaiser sporadic (13)
m Nilsson - Southworth (14)
Log10 Cumulative Flux pm-2s-1
Log10 M (g)
-2
-4
-6
-8
-10
-12
-14
-12
-10
-8
-6
-4
-2

Fig. 3

IV. Additional Studies Related to Lunar Ejecta

The previous section presented further analysis of the cosmic dust measurement from Mariner IV. This measurement shows an increase in flux between the orbits of the earth and Mars. Physically, this is not readily understood and a study was taken to consider what happens to lunar ejecta which escapes the earth's sphere of influence, thus moving in heliocentric orbits. The preliminary results of this work follows.

A. Evolution of Heliocentric Orbits of Lunar Ejecta With Masses Between 1 and 100 Picograms

A major early paper considering the application of the then known facts regarding hypervelocity impacts to meteoroids colliding with the lunar surface was presented by GAULT (1). This work indicated that there might be a large amount of the lunar surface which could leave the lunar sphere of influence. Continued efforts, both analytical and experimental, tended to lower the amount of ejecta that would be expected to have lunar escape velocities. Finally, it was possible to conduct in-situ measurements of particulate matter in selenocentric space; first, by an experiment on five Lunar Orbiters conducted during their photographic mappings of the complete lunar surface, and second, by an experiment on Lunar Explorer 35.

The results of these two experiments were very interesting. The sensors on the Orbiters were pressurized cans which lost their pressure when the walls were punctured by an impacting micrometeoroid. In general, for these sensors the threshold penetrating particles had masses in the nanogram mass range when their velocities were

heliocentric. This measurement did not show any values of dust particle flux which was different from interplanetary flux for this size range, GURTLER (2).

The LE 35 dust particle experiment detected particles of two different size ranges, ALEXANDER (3). One sensor detected particles with a threshold mass of about a nanogram. This measurement determined a flux that was essentially the same as the flux from the Lunar Orbiter experiment. The other sensor detected particles near a picogram. There were times when the picogram flux was essentially the same as that in cis-lunar and interplanetary space, ALEXANDER (4). However, there were times when the flux was significantly greater than the above sporadic flux. This happened primarily during periods of major meteor showers which had either (1) a stream-mass-component comparable to the sporadic mass plus a medium geocentric-selenocentric relative velocity such as the Geminid stream, or (2) a lower stream-mass-component, compared to sporadics, but a high geocentric-selenocentric velocity, such as the Perseid stream. During the passage of the earth-moon system through these streams for several years, ALEXANDER (5), the flux increased, as previously stated. However, the nanogram flux did not increase.

One interpretation possible from these two experiments is that there may be a component of the lunar ejecta which has escape velocity, but the lunar ejecta has an upper mass cut-off limit near a nanogram, ALEXANDER (4). Hypervelocity studies have generally shown that the velocities of the smaller ejecta particles are greater than the larger

ones, GAULT (1). However, no definitive quantitative data that has been derived from laboratory experiments existed prior to 1972. These types of measurements are very difficult to perform. GAULT (1) did give some indication of the expected flux in the picogram range from ejecta studies resulting from interpretations of hypervelocity laboratory studies of larger ejecta particles.

A decision was made to attempt a preliminary experiment designed to detect very small ejecta particles - in the micron and sub-micron range. A light-gas-gun was used to propel a primary projectile, mass of about 10 milligrams, onto a target which was a basalt like rock. Metallic targets were placed at known distances and directions with respect to the target so that ejecta particles could be impacted onto these secondary targets. The mechanical arrangement is depicted in Fig. 1. Ejecta having large ranges of masses and velocities leave the crater. However, from the results of several micro-particle hypervelocity studies, ex. NEUKUM (6) and HARTUNG (7), it is possible to recognize the signature of a high or hypervelocity micron-size particle when this particle created a crater. In the experiment, the primary projectile had a velocity of about 4 km/sec. The ejecta targets were scanned using a stereo scanning electron microscope. The results are very preliminary, but they can be used as a first estimate of the magnitude of the ejecta flux for masses less than 100 picograms. An example of micro-size ejecta caused impact craters is seen in Fig. 2. The data can be analyzed and a cumulative flux curve established for masses less than 100 picograms.

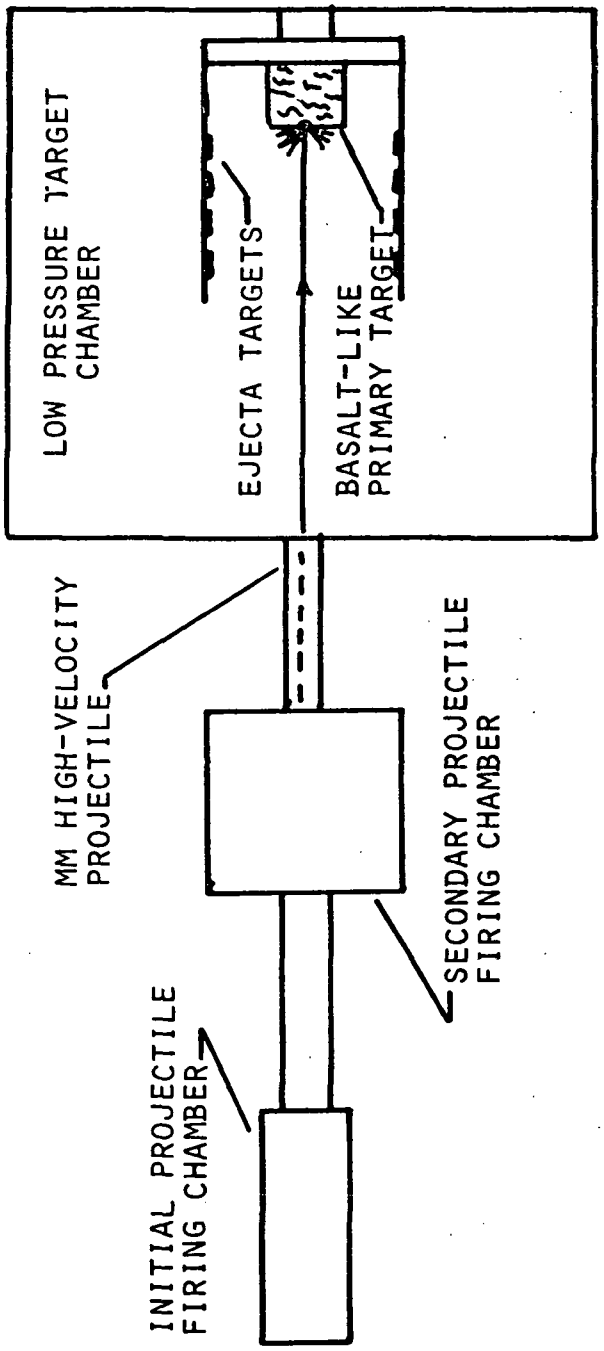

FIG. 1 LIGHT-GAS-GUN EJECTA EXPERIMENT

The data from the firing is seen in Fig. 3 in a cumulative flux curve relating cumulative number of craters, N_c, vs mass, m_p, of ejecta causing the craters. The criteria for identifying the craters as caused by hypervelocity particles and the assignment of probable diameters for the particles causing the craters is that used by NEUKEM (6). Example of data is shown below for target at 45°.

d (crater) micron	N_c	m_p pico-gram	Log N_c	Log m_p
0.5 ± 0.2	52	0.0245	1.716	-13.61
1.0 ± 0.3	12	0.1962	1.079	-12.71
1.7 ± 0.4	2	0.9642	0.301	-12.02
2.6 ± 0.5	1	3.4490	0	-11.46

Over the range of variables considered, the empirical relationship,

$$N_c = K\, m_p^{-\gamma} \qquad (1)$$

can be used to evaluate the data, since

$$\text{Log } N_c = \text{Log } K - \gamma \text{Log } m_p \qquad (2)$$

is linear with slope of $-\gamma$, and linear regression curve fitting techniques can be used to determine γ, Log K, and thus K. These quantities are found to be

$$\gamma = -0.83, \text{ and}$$

$$K = 2.76 \times 10^{-10} .$$

Therefore,

$$N_c = (2.76 \times 10^{-10})\, m_p^{-0.83}, \text{ and} \qquad (3)$$

the mass of particles for the scanning area, A_s, is

$$m_s = (2.76 \times 10^{-10}) \int m^{-0.83}\, dm,$$

$$= 1.5 \times 10^{-11} \text{ g per } A_s.$$

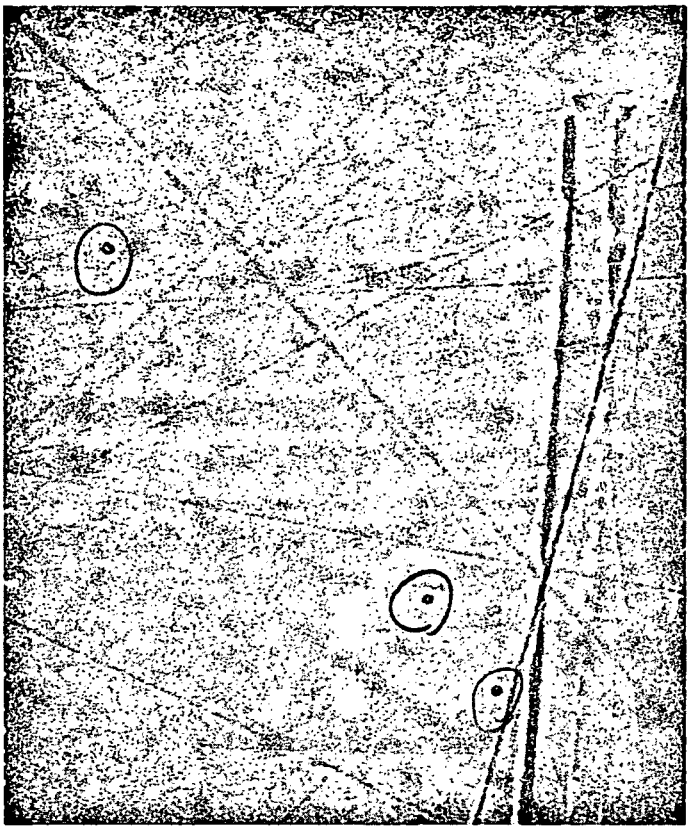

1.6 MICRONS

FIG. 2: MICRO-CRATERS FROM EJECTA CAUSED BY HIGH-VELOCITY PRIMARY PROJECTILE IMPACTING BASALT-LIKE ROCK

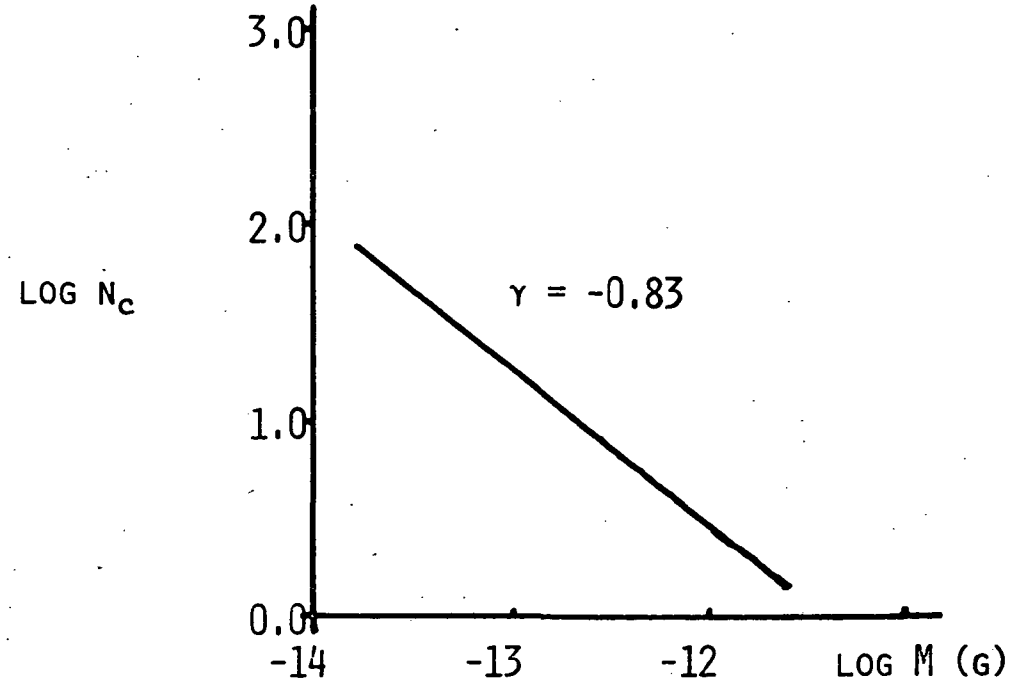

FIG. 3: CUMULATIVE NUMBER OF CRATERS VS EJECTA MASS

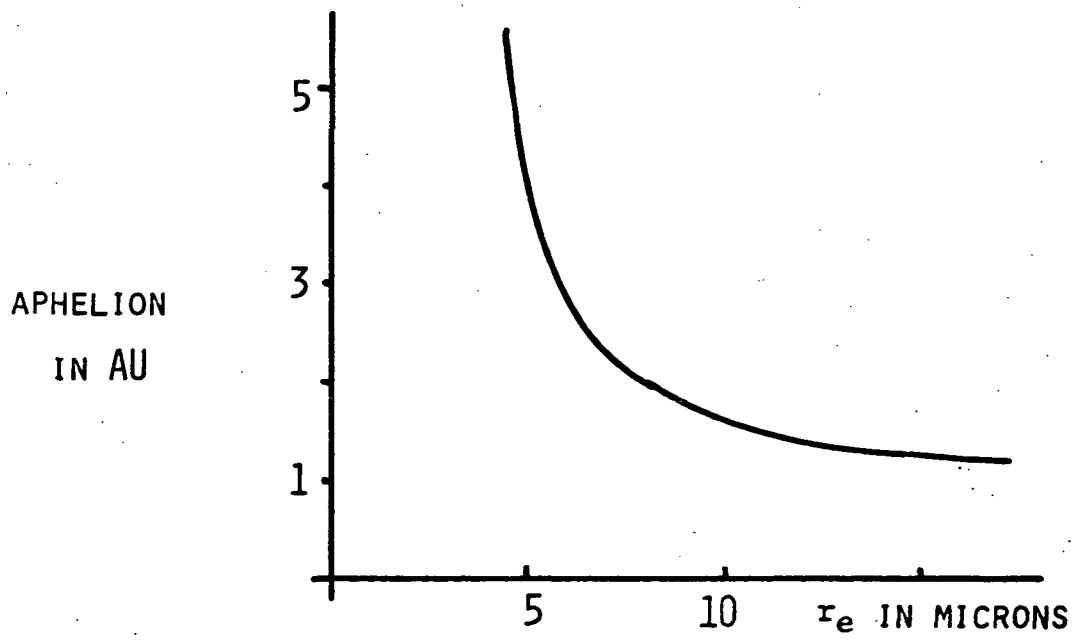

FIG. 4: APHELION DISTRIBUTIONS AS A FUNCTION OF LUNAR EJECTA RADII

A_s is 2.67×10^{-3} cm^2, therefore,

$$m_s = (1.5 \times 10^{-11} g)(2.67 \times 10^{-3} cm^2)^{-1}, \text{ and}$$

$$= 5.6 \times 10^{-9} g/cm^{-2}.$$

The preliminary studies of the various targets indicate that the m_s just derived above is quite representative of the ejecta masses over an altitude angle of 22° - 45°. Therefore, the total mass in the range of mass,

$$10^{-14} g < m < 10^{-11} g,$$

can be found by,

$$m_t = A_t m_g.$$

$$A_t = (2\pi r_t)h,$$

$$= (2\pi 11 \text{ cm})(5 \text{ cm}) = 345 cm^2.$$

$$m_t = (5.6 \times 10^{-9})(3.45 \times 10^2 g, \text{ and}$$

$$= 1.9 \times 10^{-6} g = 2 ug.$$

This is in the order of 0.05 % of the mass of the primary 4 km s^{-1} particle and agrees very well with GAULT's (8) estimate of the % of the mass of ejecta leaving the moon's sphere-of-influence with respect to the primary meteoroid mass impacting the lunar surface. The above is considered to be a low limit of the amount of ejecta having escape velocity, since the velocity of the laboratory primary particle was considerably below the mean heliocentric velocity of the interplanetary meteoroids.

ALEXANDER (9) has specifically studied the myriad orbits possible in cis-lunar space, including the effects of RP forces. It is immediately seen that RP causes a lower particle size limit cut-off of particles remaining in the solar system at a size determined by the following calculations. From,

$$v^2 = k^2(1 - \beta)(2/r - 1/a), \qquad (2)$$

where $v^2 = k^2$, $r = 1$ AU, and $a = \infty$, then

$$2\beta/r = 2, \text{ and}$$

$$\beta = 1/2 ,$$

for an ejecta particle in a parabolic orbit, the limiting orbit in the solar system. Since this ejecta particle is a lunar particle, a ρ of 3 is used in determining the mass of the particle. From ALLEN (10).

$$\beta = (5.87 \times 10^{-5})/r_p\rho_p, \text{ so} \qquad (3)$$

$$r_p = (5.87 \times 10^{-5})/\rho_p\beta \text{ cm, thus} \qquad (4)$$

$$m_p = \rho V_p = (4\pi/3\rho)\left(\frac{5.87 \times 10^{-5}}{\beta}\right)^3, \text{ and} \qquad (5)$$

$$m_p = 2.25 \text{ picograms}$$

for the particle mass at parabolic orbit limit.

The previous sub-sections have developed (1) a mechanism and rationale, based on laboratory experiments, for a preliminary determination of the amount of mass that may resonably be expected to escape the lunar-earth sphere of influence into interplanetary space, and (2) an in-situ experimentally based and analytically arrived at reason for selecting a mass range for lunar ejecta which may escape the earth-moon system. With this information, it is possible to study what happens to the lunar ejecta which is injected into interplanetary space.

As previously shown from LE 35 and the Lunar Orbiters, the lunar ejecta particles which escape the lunar sphere-of-influence have masses less than a nanogram. The lower limit mass of any significance is that near 1 picogram, as calculated in the previous sub-section. While ejecta particles with masses less than one picogram have been seen to occur, they leave on hyperbolic orbits. There is one further factor to consider. The angle of inclination, i, of most of the particles must be low because the major portion of the particles will be leaving with velocities near escape velocity. Therefore, the heliocentric velocity is not much different from that of the earth, and there can be only a small component of velocity normal to the ecliptic plane. This means that ejecta particles with aphelion distances past Jupiter have a high probability of a major pertubation which would at least remove these particles from the class of low inclination lunar ejecta particles in heliocentric orbit. Thus, it is necessary to determine the mass of particle which has a perihelion distance of one AU and aphelion near Jupiter, or a = 3.0 AU. This mass represents the real lower limit of mass for lunar ejecta that would have initial heliocentric orbits between the earth and Jupiter.

From equation (2), the value of β for a lunar ejecta particle with an a = 3 AU is found to be, 0.4, and using this value of β, the mass of the lunar ejecta particle staying inside of Jupiter's sphere-of-influence is determined to be about 4.41 picograms. Therefore the mass range for lunar ejecta in interplanetary space between 1 and 5 AU is

$$4.41 \times 10^{-12} g \leq m_p \leq 1 \times 10^{-9} g \ . \qquad (6)$$

It must be emphasized that the nanogram particle has an aphelion of only 1.056 AU, while the aphelion of the 4.41 picogram particle is 5 AU. Thus the ejecta mass range is not distributed equally in this space. The distribution would be a mixture of the initial aphelion distances combined with the in-spiraling times due to the PR effect. The aphelion distributions of the lunar ejecta are shown in Fig. 4.

The next step is to determine the possible contribution the above lunar ejecta makes to the flux of interplanetary dust particles in the solar system between 1 and 5 AU. Then, the measurement of M IV can be analyzed with respect to this additional information. To study the contribution lunar ejecta may make to the Zodiacal dust cloud, the following calculations must be made:

(1) The mass of the lunar ejecta escaping the moon and the earth sphere-of-influence,

(2) the volume of heliocentric space containing the lunar ejecta,

(3) the lifetime of these size particles in the volume of (2),

(4) the space density of dust in the volume of (2) from the lunar ejecta,

(5) the space density of dust in the volume of (2) derived from the M IV measurement and compared to the analysis of GAULT (8), and

(6) comparison of the results of items (4) and (5) above.

GAULT (8) has presented a recent study of the cumulative flux of lunar ejecta resulting from the hypervelocity impact of sporadic meteoroids onto the lunar surface. From this work, a value for the amount of lunar ejecta mass below a nanogram is obtained. In previous sub-sections, arguments were presented to support the concept that lunar ejecta with masses smaller than a nanogram would escape the moons sphere-of-influence. GAULT (8) found the mass of ejecta below a nanogram to be 2×10^{-1}g cm^{-2} MY^{-1} (MY = million years), or $m_a = 2 \times 10^{-7}$ g cm^{-2} y^{-1}. It is this mass that is proposed to be lunar ejecta which is injected into heliocentric space. The preliminary laboratory experiment already described supports this figure, though the GAULT (8) value may prove to be a little low as the result of future experiments.

Next, the area, A_1, of the lunar surface is found from

$$A_1 = 4\pi r_1^2, \qquad (7)$$

$$= 4\pi(1.738 \times 10^8 \text{ cm})^2, \text{ and}$$

$$= 3.9 \times 10^{17} \text{ cm}^2.$$

Therefore, the total mass leaving the moon's sphere-of-influence is

$$m_t = m_a A_1, \qquad (8)$$

$$= 2 \times 10^{-7}\text{g cm}^{-2}\text{ y}^{-1} \times 3.9 \times 10^{17} \text{ cm}^2, \text{ and} \qquad (8)$$

$$= 7.8 \times 10^{10} \text{ g y}^{-1}.$$

The heliocentric velocity of these particles at injection will be very little different from 29.8 km s^{-1}. An increment of velocity of about 0.5 km s^{-1} perpendicular to the ecliptic plane will result in a lunar ejecta particle leaving the earth's sphere-of-influence with an inclination angle of only 1°. At a distance of 1.6 AU, this particle will be out of the ecliptic plane by only about 1×10^{-2} AU. Thus, the volume of heliocentric space which contains the major portion of the lunar ejecta in the range of the measurement of M IV is essentially a cylinder with an inner radius, r_i, of 1.1 AU, an outer radius, r_o, of 1.6 AU, and a thickness, t, which averages about 1×10^{-2} AU. The volume of this space is

$$V_{cld} = \pi(r_o^2 - r_i^2)t \ , \qquad (9)$$

$$= (3.14)(1.6^2 - 1.1^2)(1 \times 10^{-2}) \ AU^3 \ , \text{ and}$$

$$= 1.4 \times 10^{38} \ cm^3.$$

The next essential information needed is the lifetime of these particles in the above volume. That is, the in-spiraling time back to 1 AU. What happens after the particles arrive at 1 AU will be discussed in a following section. For these particles, the orbits will be essentially circular on into the inner most parts of the solar system after arriving at 1 AU. Thus, the WYATT-WHIPPLE (11) type calculations can be used (again, neglecting the earth, for the moment) and the portion of time required for particles to move back to 1 AU is found, at an average, to be in the order of 1000 years.

It must be remembered that the largest of these particles have the smallest values of semi-major axis, and the smaller ones the largest values. This means that the actual PR times are not greatly different, since the smaller particles have the further distances to travel in returning to the region of injection at 1 AU. The significant fact is that the lunar ejecta injected into this volume has an average lifetime of about 1000 years in the volume.

The next step is to determine the space density, ψ_{sd}, of lunar ejecta in this cylinder. The total mass per year injected into the above volume was earlier found to be 7.8×10^{10}g. For a time period of 1000 years, this would then be a total mass, m_t, of 7.8×10^{13}g. The spatial density, ψ_{sd}, can be determined by,

$$\psi_{sd} = m_t \, V^{-1} , \qquad (10)$$

$$= (7.8 \times 10^{13}\text{g})(1.4 \times 10^{38} \text{ cm}^3)^{-1}, \text{ and}$$

$$= 5.6 \times 10^{-25}\text{g cm}^{-3} .$$

The spatial density of this dust is now found from the measurement of M IV. The M IV results are expressed in a cumulative flux curve presented in Fig. 5. The equation for this cumulative flux, ϕ_c, is

$$\phi_c = (6.9 \times 10^{-12}) \, m^{-0.64} \quad \text{pm}^{-2}\text{s}^{-1} . \qquad (11)$$

The mass of these particles over the incremental mass range of

$$10^{-12}\text{g} < m < 10^{-9}\text{g} ,$$

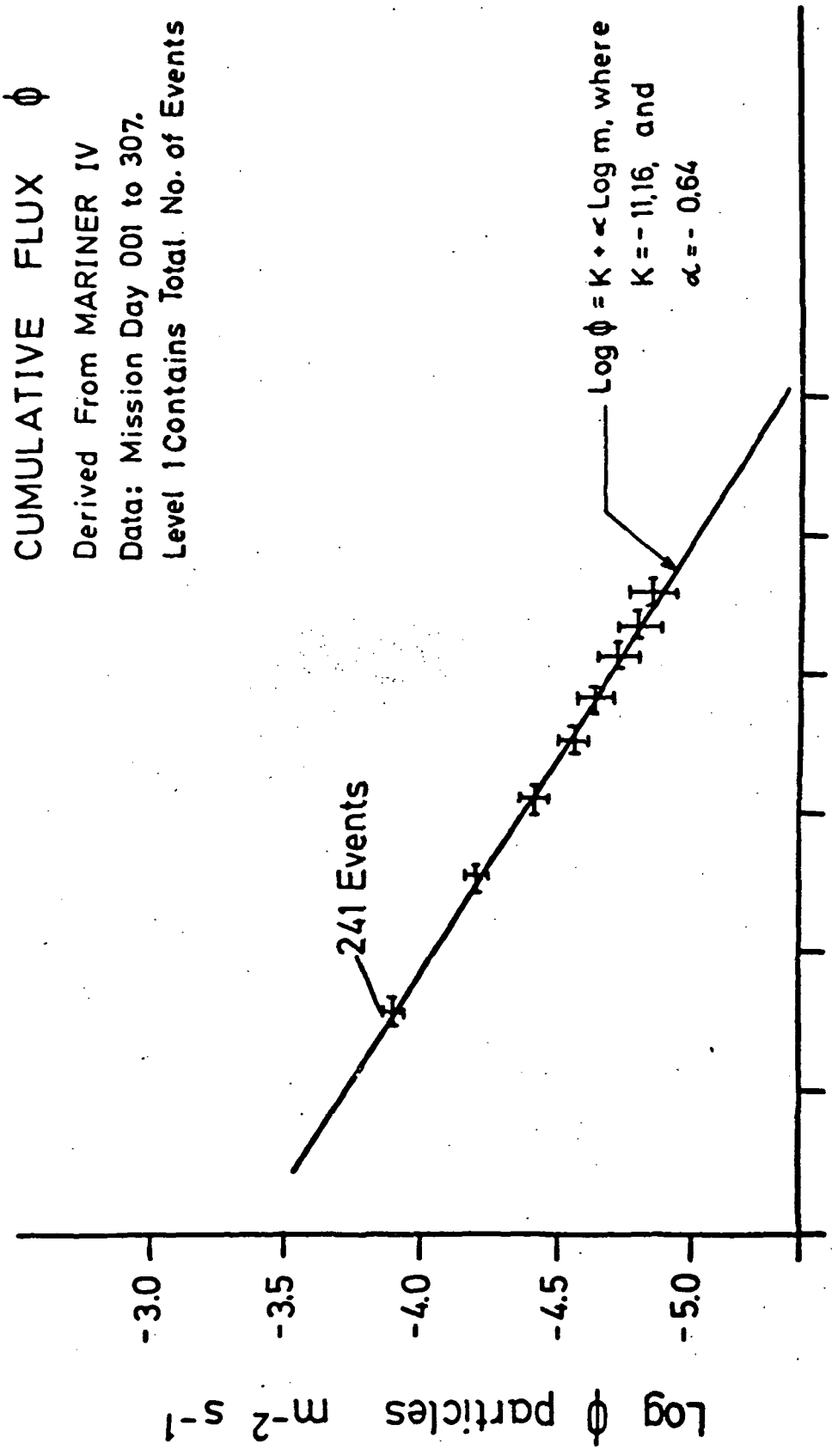

FIG. 5: AVERAGE CUMULATIVE FLUX-MASS DISTRIBUTION CURVE FROM MARINER IV
R = 1.0 AND 1.6 AU

can be obtained from

$$m_c = (6.9 \times 10^{-12}) \int_{10^{-12}}^{10^{-9}} m^{-0.64}\, dm, \text{ and} \qquad (12)$$

$$m_c = 1.01 \times 10^{-14} \text{ g m}^{-2} \text{ s}^{-1} .$$

Spatial density can then be determined from

$$\psi_{sd} = m_c \, \bar{v}_p^{-1} \text{ , where} \qquad (13)$$

$\bar{v}_p$ is the mean heliocentric velocity of these particles in this volume. This velocity is near 25 km s^{-1}, which is the velocity used. Therefore,

$$\psi_{sd} = (1 \times 10^{-18} \text{ g cm}^{-2} \text{ s}^{-1})(2.5 \times 10^{6} \text{ cm s}^{-1})^{-1}, \text{ and}$$

$$\psi_{sd} = 4 \times 10^{-25} \text{ g cm}^{-3}.$$

From this value of ψ_{sd} derived for the M IV measurement, the mass of these M IV particles in this volume is given by

$$M_{cld} = \psi_{sd} \, V_{cld}, \qquad (14)$$

$$= (4 \times 10^{-25} \text{ g cm}^{-3})(1.4 \times 10^{38} \text{ cm}^{3}), \text{ and}$$

$$= 5.6 \times 10^{13} \text{g} .$$

Other such calculations were made using GAULT's (8) distribution for interplanetary space. The cumulative flux used by GAULT (8) was based on a number of measurements. These measurements were made primarily near the earth. However, the results are interesting.

From GAULT (8),

$$\phi_c = 1.45\ m^{-0.47}\ p\ cm^{-2}\ MY^{-1}, \qquad (15)$$

$$m_c = 1.45 \int m^{-0.47}\ dm, \text{ and}$$

$$= 4.55 \times 10^{-5}\ g\ cm^{-2}\ MY^{-1}, \text{ or}$$

$$= 1.45 \times 10^{18}\ g\ cm^{-2}\ s^{-1}\ .$$

For spatial density, using the same method as M IV,

$$\psi_{sd} = 5.8 \times 10^{-25}\ g\ cm^{-3}\ .$$

Finally, the cloud mass is

$$M_{cld} = 8.1 \times 10^{13}\ g.$$

This result compares quite favorably with that obtained from the M IV measurement.

However, the significant factor is the comparison of the dust cloud mass determined from the M IV measurement, GAULT (8) analysis, and the lunar ejecta injected into this volume. The first two had a cloud mass value between $(4 - 8) \times 10^{13}$ g, while the lunar ejecta calculations had a value near 8×10^{13} g injected over a 1000 year period. Since this value, including the lifetime estimates, is very similar to the first two results, the contribution possible is seen to be significant. The overall comparisons are made in the next section.

4. Gegenschein and the Mariner IV Measurement

The M IV spacecraft traveled a path from earth to Mars which was essentially in the ecliptic plane. The detector plate was oriented in such a manner that it was most sensitive in terms of velocity and detection solid angle to particles of low inclination and low values of eccentricity. Thus, M IV detected particles which were most likely those comprising the major portion of the particles making up the Gegenschein. The Gegenschein measurements provide the information which prove the fact that the Gegenschein is not the result of only lunar ejecta. ROOSEN (12) has recently conducted extensive studies regarding the Gegenschein and presents strong evidence that the Gegenschein is not a phenomenon which is near the earth. It has been shown, in a previous sub-section, that lunar ejecta would not concentrate near the earth, but due to RP, it would be in a heliocentric ring outside the orbit of the earth. However, this ring would have a very narrow thickness. The observations reported by ROOSEN (12), do not show a sharp peak of intensity very near the ecliptic plane. This would mean that the lunar ejecta was not the only contributor to the complete Gegenschein but it does not rule out that the lunar ejecta is possibly the major enhancement factor of the peak intensity within $\pm$ 2° of the ecliptic plane. Further remarks are reserved for the last section. This work suggests future studies which are beyond the scope of the present effort, but pertinent to understanding the Gegenschein.

B. Relationship of Mariner IV Measurement to Zodiacal Dust and Gegenschein

It is generally accepted that the dust comprising the zodiacal dust cloud comes from comets and grinding-up processes occuring in the asteroid belt. Whipple (14), for example, finds that comets Encke and Halley provide sufficient mass to account for the primary portion of dust in this cloud. In addition, studies concerning the grinding-up of asteroidal materials have been presented by Dohnany (13) and Whipple (14). At the present time it is not possible to arrive at a firm decision regarding the relative efficiency of these two sources, but it is most likely that the origin of the majority of the dust is a combination of both sources.

The preceding remarks are general in terms of the overall zodiacal dust cloud. In studying the Mariner IV measurement, considerations of the data and the ground-based observations of the Gegenschein were found to be important and are presented below.

The Mariner IV sensor plate was most efficient in detection of particles with very low inclinations. The main reason is that the effective impact area of the sensor simply decreases for higher inclination particles since the vector $\bar{n}$ was always low with respect to the ecliptic plane. Secondly, the acoustic transducer was responsive to a mechanical excitation which was related to the impulse delivered to the impact plate by the micro-particle hypervelocity impact. Since this impulse is a

vector quantity, then the detector array was most sensitive to particles of low inclination. Therefore, while the impact plate was reasonably sensitive to particles over a fairly wide range of inclination, i,

$$0° < i < 45°, \text{ or}$$

$$135° < i < 180°, \text{ the}$$

detection efficiency is greatest for the lowest inclination particles. This means that the M IV sensor was most efficient for detection of Gegenschein particles. A comparison of the M IV measurement and the most recent work regarding the ground-based Gegenscheinobservations is the next step.

Roosen has conducted the most recent in-depth Gegenschein measurements. A representative summary of his works are found in Roosen (12), (16), (17), and (18). The primary Roosen results relative to the Gegenschein and the M IV measurements are as follows:

(1) the Gegenschein maximum brightness was found to be exactly at the anti-solar point;

(2) the Gegenschein maximum was found to be exactly in the ecliptic plane; and

(3) the dust particles responsible for the Gegenschein had to be quite far from the earth, or essentially in a heliocentric rather than a geocentric cloud.

Whipple (12) and Roosen (15) have pointed out that consideration of asteroidal debris as the sole source of Gegenschein particles is contrary to the Roosen observations, since the mean mass of the known asteroids is not exactly centered in the sun-earth ecliptic plane. However, material from a source in the ecliptic plane would be distributed around this plane. Therefore, if the dust particles near the ecliptic plane are the result of a combination of asteroidal debris and lunar ejecta, then the ground-based observations of Roosen should exhibit the following characteristics:

(1) a maximum at the anti-solar point and exactly in the ecliptic plane if the lunar ejecta particles are present in any significant degree; and

(2) a slight asymmetry with respect to the ecliptic plane for i's greater than about $\pm 2°$ if the asteroidal debris also makes a measureable contribution to the Gegenshein.

In studying Roosen's (12) data, a very important fact is seen which is a strong indication of no. 2 above. The brightness vs. declination angle from the anti-solar data clearly shows an asymmetrical distribution for data greater than $\pm 2°$ of the anti-solar point. The brightness data indicates a probable dominance of particles with slight positive inclinations. The above indicates a model for the Gegenschein that contains asteroidal debris with lunar ejecta superimposed upon it in the region of the ecliptic plane. Of course, there is also a mixture

of some debris from the cometary sources, but the amount in this very small volume of the overall Zodiacal Dust cloud is small.

The final topic to discuss is the radial distribution of the dust particles as measured by M IV and the distribution indicated by the ROOSEN (12) Gegenschein observations and analyses. In the data section of this work, it was shown that the CF-MD from the M IV measurement appears to increase as the heliocentric range increased. Near the orbit of Mars ϕ_c decreased, but not to the level of that near 1 AU. Normal distribution of particulate matter revolving around an object such as the sun will exhibit a higher concentration of the particles as the distance to the sun decreases. The spatial density as a function of heliocentric range, R, is modified by the various forces acting on the particles (other than gravitational) causing them to change their orbits (such as PR, RP, and the others). In any event, through, the variation of ϕ_c as a function of R is of the form R^{-n}. However, the measurement of M IV gives a positive value of n. As a first consideration, this statement does not make sense from a physical viewpoint. However, it must be remembered that this is a measurement within a very small volume of the overall Zodiacal Dust cloud. If there are any forces or events which relate primarily to phenomena only effecting this zone, then this apparent anamolous information does not relate to the overall dust cloud, but only to the region where the measurement occurred.

SOUTHWORTH (19) and BANDERMANN (20) have shown that if the interplanetary dust is due to cometary debris, then PR drag causes the dust concentration to vary with values for n of -1 for R < q and -2.5 for R > q. Thus if WHIPPLE'S (14) calculations regarding comets Encke and Halley are used, then the present dust cloud would be expected to follow a $R^{-2.5}$ distribution at 1 AU and out since q for both comets is < than 1. That part of the dust cloud that is the result of grinding up processes in the asteroid belt would have a radial distribution of R^{-1} at 1 AU. With the above facts in mind, ROOSEN (12) determined that he should be able to detect the shadow of the earth in the brightness measurements of the Gegenschein for either value of n with -2.5 being the easiest to detect. He did not find any depression in the brightness observation at 0° declination from the antisolar point. The conclusion ROOSEN (12) reached was that the Gegenschein is the result of back-scatter from a heliocentric dust cloud that is most likely asteroidal material with the major portion of this cloud quite removed from 1 AU. As previously stated, the major problems with the above is that ROOSEN'S (12) photometric measurements show (1) the maximum brightness to be exactly at the anti-solar point and (2) in the ecliptic plane. This should not be the case if the debris were asteroidal alone. It has already been proposed that lunar ejecta added to asteroidal debris could possibly account for the maximum to be in the ecliptic plane. In addition, ROOSEN (12) should have been able to detect the earth's shadow even for R^{-1}, and he

did not find it. If a mechanism exists which alters the value of n to values significantly less than -1, then the shadow problem would not exist.

One possible mechanism which might alter the effective value of n has been presented by SCHMIDT (21). He showed that particles arriving at the earth's sphere-of-influence in essentially circular orbits and small enough to be affected by PR effect may have the steady inward motion due to PR disturbed by the earth's gravitational action and the perihelion distance increased. SCHMIDT (21) demonstrated that when this interruption caused e to increase to values over 0.07, then the inward drift is barely disturbed. The general conclusion of SCHMIDT (21) was that there could be some concentration of particles in a heliocentric ring outside the earth's orbit with a space density increase by as much as a factor of 5. It is interesting to note that the increase in ϕ_c from M IV is about a factor of 3.5, with this value being reached around 1.35 AU. This value of R is too high for the gravitational scattering presented by SCHMIDT (21). However, his interesting work has been mentioned to demonstrate that there are factors which alter the apparent radial distribution when measured near the ecliptic plane, as well as a possible 1 AU source factor.

The previous chapters have presented the M IV measurement and the numerous factors surrounding the measurement and data analysis. The instrument was not an extremely sophisticated device and care

has been taken not to try and obtain more information from the results than is possible. The analysis effort has raised several very interesting questions that should be pursued in future research efforts. Because of M IV and LE 35 results, laboratory studies of the mass and velocity distribution of micro-sized ejecta resulting from hypervelocity impact is needed; a further look at the last Gegenschein measurements, especially with regards to the possible need for more ground-based observations (it is noted that Pioneer 10 results may negate this observation); and many theoretical problems need to be pursued, starting with the possible heliocentric ring as seen by M IV, pointed out by SCHMIDT (21), and presented as a major explanation of the Gegenschein by ROOSEN (12) from his observations and analyses of the Gegenschein.

REFERENCES

(1) Gault, D. E., E. M. Shoemaker, H. J. Moore; NASA Report TND-1767 (1963)

(2) Gurtler, C. A., G. W. Grew; Science 161, 462 (1968)

(3) Alexander, W. M., C. W. Arthur, J. D. Corbin, J. L. Bohn; Space Research X, 252 (1970)

(4) Alexander, W. M., C. W. Arthur, J. L. Bohn; Space Research XI, 279 (1971)

(5) Alexander, W. M., C. W. Arthur, J. L. Bohn, J. H. Johnson, B. J. Farmer; Space Research XII, 349 (1972)

(6) Neukem, G., F. Horz, J. B. Hartung, D. A. Morrison; Proc. Fourth Lunar Sci. Conf., Pergamon Press (1973), in press

(7) Hartung, J. B., F. Horz, K. F. Aitken, D. E. Gault, D. E. Brownlee; Proc. Fourth Lunar Sci. Conf., Pergamon Press (1973), in press

(8) Gault, D. E., F. Horz, J. B. Hartung; Proceedings of the Third Lunar Conference Volume 3 (edited by D. R. Criswell) 2713 (1972)

(9) Alexander W. M., C. W. Arthur, J. L. Bohn, J. C. Smith; to be published 1973 in: Space Research XIII

(10) Allen, C. W.; Astrophysical Quantities, Athlone Press, 157 (1964)

(11) Wyatt, S. P., F. L. Whipple; Astrophys. J., 111, 134 (1950)

(12) Roosen, R. G.; Physical Studies of Minor Planets (edited by T. Gehrels), 363 (1971)

(13) Dohnanyi, J. S.; Icarus 17 1 (1972)

(14) Whipple, F. L.; The Zodiacal Light and the Interplanetary Medium (edited by J. L. Weinberg), NASA SP 150, 409 (1967)

(15) Whipple, F. L.; Physical Studies of Minor Planets (edited by T. Gehrels), 389 (1971)

(16) Roosen, R. G.; Icarus, 9, 429 (1968)

(17) Roosen, R. G.; Icarus, 13, 184 (1970)

(18) Roosen, R. G.; Review of Geophysics and Space Physics, 9, no. 2, 275 (1971)

(19) Southworth, R. B.; Ann. N. Y. Acad. Sci., 119, 54 (1964)

(20) Bandermann, L. W.; Ph.D. Dissertation, University of Maryland (1968)

(21) Schmidt, T.; The Zodiacal Light and the Interplanetary Medium (edited by J. L. Weinberg), NASA SP 150, 333 (1967)

V. Concluding Remarks

The data from the three missions has produced significant information in several areas concerning the interplanetary dust complex. These are listed in a summarized manner below:

A. Mariner IV showed a reliable measurement with no evidence of noise. The cumulative flux from this experiment and the resultant cumulative flux-mass distribution which is derived from a single experiment is in very good agreement with (1) the zodiacal light model of Geise, Type II, (2) the extension of the penetration flux, and (3) most importantly with the flux as seen from Pioneer 8 and 9. The increase of flux between the orbits of earth and Mars is felt to be real and presents questions that will only be resolved by further studies.

B. The OGO III measurement provided the initial in-situ measurement of velocity of a dust particle and the cumulative flux data point of 0.5 picogram particles.

C. The Lunar Explorer 35 experiment provided a study of the dust particle flux in selenocentric space over a period of several years. There is some evidence that ejecta particles from the lunar surface whose masses were in the order of a picogram were detected. However, this is not directly measurable and the evidence is not conclusive.

D. The various considerations to the analysis of data from these experiments indicate that immediate studies should continue to:

1. Analyze in greater depth the initial study of micron sized ejecta leaving the earth in the system and moving into heliocentric space.
2. Attempt to attain more laboratory data regarding the mass-velocity distribution of minute ejecta from hypervelocity impacts.
3. Analyze the data from Lunar Explorer 35 and OGO III to look for data that is cyclic in nature, even though the periods might be quite long. (There is some evidence

of such occurances in the Lunar Explorer 35 data when periods of 45 or 50 days are considered. There is evidence from Pioneer 8 and 9 that there are very small particles on nearly parabolic to hyperbolic orbits coming from near the sun. The two experiments listed above may have measured some of these particles and additional study might show this.)

VI APPENDIXES

A. I- Lunar Explorer 35

B. II - Papers and Publications, 1968 - present

A

APPENDIX I

GENERAL DESCRIPTION OF SYSTEM: Lunar Explorer 35

The basic sensor signals are derived from two different sensor groups. One set of sensor signals is derived from sensors within a cylindrical tube into which dust particles enter from space. The tube sensors are located near the ends of the tube, spaced by fixed known dimensions. This physical spacing is utilized to enable a time of flight (TOF) measurement of a dust particle. The other sensor group is associated with a circular plate of large area exposed on the AIMP spacecraft exterior.

In event of a particle impact with either sensor system (tube or plate), the signals are amplified, processed and the necessary analog data converted to digital form. The digital data are then stored in a specific readout order in shift registers within the instrumentation. At the appropriate readout interval the data are shifted out into the spacecraft (S/C) telemetry system for further processing and transmission.

The shift registers are arranged to only change stored data in event of a new data event. During readout the data are recirculated in the registers so that the same data pattern continues to be read out in each particular data frame until new data are received. This is of significance when there are sources of data error due to land based systems in the data link to the experimenter and when the data rate is low as in this type of experiment. This operation is in accordance with requirements in the experiment functional specifications

In event of two data events in one sensor system between two successive telemetry readouts for that sensor system, the data of the second event are not processed and the first event data for that sensor group are retained in the appropriate section of the shift registers. The exception to this is the count data of the accumulative hit event counters which are triggered for each event. From the data readout of these "hit" accumulators it can be determined if such a double event occurred between successive readouts for a particular sensor system.

DESCRIPTION OF OUTPUT DATA.

General.

There are four channels of output data. They are referred to as Level A through Level D. In all four channels, the most significant digit is read out first.

The inter-binary cross-coupled steering in the Shift-Register (S/R) is arranged to recirculate the data back into the binaries, as it is being shifted out.

The TOF, M_T PHA, Mp PHA, M_T ACC, Mp ACC are all combined counter and Shift-Register binaries.

The SA string consists of five counters and five separate shift-register binaries. The data will be transferring from the counters to the S/R at all times except (a) when the counter is still counting, and (b) during readout.

The Status/RFI Binary is a shift-register binary only. Its state is controlled by sets and resets.

Level "A" Output.

All six binaries in this string are the binaries for the Time-of-Flight (TOF). The maximum count is 63.

Level "B" Output.

The first five bits read out are the Solar Aspect (SA) data. The maximum count is 31.

The last bit to be read out will be the Status/RFI binary. This binary monitors RFI or the status of the A_T and B_P Sensors. A logical 1 indicates RFI or a shorted sensor (depending on what is being monitored).

Level "C" Output.

The first three bits read out are the data in the M_T PHA binaries. These tell the peak amplitude of pulses in one of the input channels connected to the tube sensor, the M_T channel. The maximum count is 7.

The second set of three bits (fourth, fifth, and sixth) to be read out are the M_P PHA data. Similar to the M_T PHA data, these give the peak amplitude of pulses in the M_P channel, a plate sensor input channel. The maximum count is 7.

Level "D" Output.

The first three bits read out are the data in the M_T ACC binaries. This gives the number of hits in the M_T channel. The maximum count is 7, but the binaries are never reset. So, they will count on to 0 and start counting up again, except for blocked time during INHIBIT intervals or when completing a measurement.

The second three bits read out are the data in the M_P ACC binaries. This tells the number of hits in the M_P channel. Like the M_T ACC above, maximum count is 7, and the binaries can count continuously except for blocked time during INHIBIT intervals or when completing a measurement.

EXPLANATION OF OUTPUT DATA.

TOF (Level "A" Output).

The time of flight (TOF) measurement is made by the A_T and B_T channels. Logarithmic compression is used in the analog-digital conversion (A-D/C). A capacitor is charged by a constant current for the time equal to the TOF, then at a later time it is allowed to discharge through a precision resistor. From the start of discharge until the voltage reaches a predetermined level, a gated-free-running clock (GFR) is allowed to free-run and drive the TOF counter. Therefore, the number of counts is proportional to the logarithm of the TOF. The minimum for FULL SCALE (63 counts) is 50 μsec.

Solar Aspect (First Five Bits Read Out In Time From Level "B" Output).

The Solar Aspect (SA) GFR is allowed to start free-running and driving the SA counter whenever there is a hit. This is true for a tube-sensor hit, a plate-sensor hit, or a simulated hit from the Calibration Generator. However, in normal operation (no CAL signal) the tube-sensor hit has precedence. The logic is so arranged that (a) after a tube-hit has started the SA GFR, it cannot be restarted by a plate hit until after the next readout of data; and (b) if a plate-hit has started the GFR, a tube-hit that occurs after that but before the next readout will reset the SA counter binaries and the SA GFR will now be putting in the data for the tube-hit. The GFR continues to operate until either the full-scale signal or the Solar Aspect signal occurs. The Solar Aspect signal indicates the SA sensor has sighted the sun.

If the GFR (and the counter) are still in the process of measuring SA when the Counter Inhibit Signal arrives (160 ms before readout and 160 ms after the Inhibit Signal which blocks all input channels) the SA Shift Register (S/R), having been reset by the hit, will read out all zeros. The data in the counter is transferred to the S/R by DC-SET to the S/R binaries at all times except when (a) the GFR is still operating and the counter still counting and (b) the Counter Inhibit Signal (preparing for readout) occurs. There are two possible marginal areas. First, if a tube hit occurs after a plate hit and the SA GFR is still operating there will be an ambiguity of 1 count, because the tube hit will allow the GFR to keep operating but will reset the counter to all zeros. Secondly, if counting is still in process when the Counter Inhibit Signal occurs, but counting ends before the end of readout (so that all input channels are again open for new hits), and a new hit does occur before the next readout, the new hit will have its SA data measured and the first hit will not have any SA data. However, both of these occurrences are unlikely.

The maximum SA that can be measured before the Full-Scale signal occurs is 3.0 sec. at room temperature. This means that if the Spacecraft rotates at less than 20 rotations per minute, the counter could reach full-scale.

The SA GFR period is 100 milliseconds. The maximum count is 31.

Status/RFI Binary (Sixth Bit of Level "B" Output). (See "F", Pg. 6)

For normal readouts (those not preceded by calibration) the Status/RFI binary indicates whether an RFI indication occurred at any time since the last readout. If RFI did occur, the Status/RFI bit will be a logical 1. The binary is reset to zero after each readout. For calibration readouts, the Status/RFI bit indicates either (a) the status of the A_T sensor, or (b) the status of the B_P Sensor, or (c) the occurrence of an RFI indication. Which of these is being indicated may be determined from the calibration level, as described in section IV.F. When RFI is being monitored during a calibration readout, the Status/RFI bit should always be a logical 1, because an RFI indication is simulated during calibration. When the A_T or $B_{\bar{P}}$ sensor status is being monitored during a calibration readout, the Status/RFI bit will be a logical 1 only if the respective sensor is shorted.

M_T PHA (First 3 Bits Read Out In Time From Level "C" Output).

When the M_T channel receives a hit, the 3KC amplifier drives the peak-catch and hold circuit which captures the peak voltage from the amplifier. Later the capacitor which stored the peak is discharged through a precision resistor. The M_T PHA GFR is gated on from the start of the discharge until the voltage reaches a predetermined level. Therefore, the analog to digital conversion is logarithmically compressed, giving a greater dynamic range. The number of counts is proportional to the logarithm of the peak voltage. The minimum peak voltage that will give 1 count in the output is 143 μv . The minimum peak voltage that will give a full scale reading (7 counts) is 5.98 mv. Both of these values are at the input to the M_T amplifier.

M_P PHA (4th, 5th, 6th Bits Read Out In Time From Level "C" Output).

Whenever there is a coincident hit in the B_P and M_P channels, two things happen: (a) the 3 M_P PHA binaries in the S/R are reset to zero, and (b) the amplifier drives the peak-catch and hold circuit, which captures the peak. Later the capacitor which held the peak is discharged through a precision resistor. The M_P PHA GFR is gated on from the start of the discharge until the voltage reaches a predetermined level. Therefore, in this circuitry, as in the M_T PHA, logarithmic compression is used in the A-D/C; the number of counts is proportional to the logarithm of the peak voltage. The minimum peak voltage to give 1 count is 67 μv . The minimum peak to give a full scale reading (7 counts) is 3.11mv. Both of these values are at the amplifier input.

If there is an M_P hit but no B_P hit, then there will be no M_P PHA measured. However, the M_P ACCUMULATOR will indicate a hit. The function of the B_P channel is to indicate if a true hit has occurred (a coincident hit) or if the M_P channel (a crystal sensor and a 100 KC tuned amplifier) was falsely triggered by acoustical or mechanical noise. If there is an M_P "hit" but no B_P hit, it probably was this noise. If there is a B_P hit, but no M_P hit, nothing occurs in the data measurement/storage sections since the "coincident" circuitry does not operate for just a B_P hit.

M_T Accumulator (First 3 Bits Read Out In Time From Level "D" Output).

These three binaries in the S/R record the total number of hits received by the M_T amplifier (by advancing 1 count each hit) either from the sensor or from the CALIBRATION GENERATOR. These binaries are never reset and they will record multiple hits prior to a readout. That is, if two or more hits should occur at the M_T channel between readouts, the M_T PHA, Solar Aspect, and TOF counters would have data for only the first hit. However, the M_T ACCUMULATOR will record every hit. After an M_T hit, the input to the Peak-Catch and Hold circuitry is blocked for 0.5 seconds to allow the slowly damped wave (in the case of a mechanical vibration) from the 3KC amplifier to die away. This is to prevent extra triggers to the M_T Accumulator.

Mp Accumulator (4th, 5th, 6th Bits Read Out In Time From Level "D" Output)

These three binaries in the S/R record the total number of hits received by the Mp amplifier (by advancing 1 count each bit), either from the sensor or from the CAL GENERATOR. These binaries are never reset and will record multiple hits in the Mp channel between readouts. These binaries are identical to those of the M_T ACC in design and function.

RELATED LOGIC.

RFI Block.

Whenever the RFI Sensor detects RFI above a predetermined threshold, the RFI circuitry blocks all input channels (A_T, B_T, Bp, Mp) except M_T. This is to prevent the RFI from triggering the extremely fast channels. The delay time thru the RFI BLOCK circuitry is very short to enable the blocking action to take place before false triggering could occur. The same signal that initiates the RFI BLOCK will show RFI present on the STATUS/RFI binary (BIT 6 of Level "B" Output) if RFI occurs, or if RFI Cal occurs.

Tube Block.

After one hit has occurred in any tube channel (A_T, B_T, or M_T) and until the next readout is over, the TUBE BLOCK signal is arranged to keep subsequent hits from being processed (except for the M_T ACCUMULATOR, which still will count multiple hits). Also, the TUBE BLOCK will block new data during readout. At the end of readout, the block is removed so that new hits can be processed.

Plate Block.

This is analogous to the TUBE BLOCK in that it blocks the Bp and Mp channels (a) after a Bp-Mp coincident hit and before the next readout, and (b) during readout. A Bp or Mp hit alone (no coincidence) will not initiate the PLATE-BLOCK.

Inhibit Signal.

This signal prepares the circuits for readout. It blocks all of the input channels. It goes down at the end of readout and takes away the TUBE BLOCK and PLATE BLOCK. This allows the channels to accept hits again.

Counter Inhibit Signal.

This signal occurs 160 ms after the INHIBIT SIGNAL. This signal will stop all activity in the logic and A-D/C sections 160 ms after the inputs have been blocked. This allows any hits which might have been received just before the INHIBIT SIGNAL to have an extra 160 ms to be processed before input signal processing is stopped for purposes of readout.

Cal Storage and Control.

The logic is arranged so that if a CAL SYNC signal comes either (a) during readout or (b) before a "new" hit's data has been read out, the CAL SYNC signal is stored until after readout. Then the appropriate CAL signals (from the CAL GENERATOR) are injected into all the amplifiers. There are two levels of CAL, an upper level and a lower level. That means there are two distinct patterns and each level is repeated. For example, assume CAL SYNC occurs, and CAL LEVEL #1 goes into all the amplifiers. The next time CAL SYNC occurs, CAL LEVEL #1 will be put in again. The third and fourth times, CAL LEVEL #2 will be put in. This pattern then repeats itself, continuously.

The A_T Sensor and the Bp Sensor are examined during CAL. The first time CAL LEVEL #1, the lower level (identifiable because of the lower TOF count) is put into the amplifiers, the A_T Sensor Status is monitored. The second time CAL LEVEL #1 goes in, the Bp Sensor Status is shown. The first time CAL LEVEL #2 and the second time CAL LEVEL #2 goes into the amplifiers, RFI Cal is monitored.

CAL LEVEL	#1 (Lower)	#1 (Lower)	#2 (Upper)	#2 (Upper)
Data in Status/RFI Binary	A_T Sensor Status [0 = Unshorted, 1 = Shorted]	Bp Sensor Status [0 = Unshorted, 1 = Shorted]	RFI CAL [This Bit is a Logical 1 for RFI Cal]	RFI CAL

——— TIME SEQUENCE OF CALIBRATION EVENTS ———→

GENERAL INFORMATION ABOUT THE SHIFT REGISTERS.

Combined Counter - Shift Register.

The TOF, Mp PHA, M_T PHA, Mp ACC, M_T ACC are all combined counter and shift-register binaries.

Separate Counter - Shift Register.

The SA binaries have five counter binaries and five separate shift register binaries. The data will be transferring from the counters to the

shift registers at all times except (a) when the counter is still counting, and (b) during readout.

The Status/RFI Binary is a shift-register binary only. Its state is controlled by sets and resets.

Data Recirculation.

The inter-binary cross-coupled steering is arranged to recirculate the data back into the binaries, as it is being shifted out. This is a valuable feature in any system with land-based error sources and a low data-rate.

DATA FORMAT

	First Bit Shifted Out	Identification of Data Output Bits → TIME →				Last Bit Shifted Out
	MOST SIGNIFICANT TOF BIT					LEAST SIGNIFICANT TOF BIT
Level A:	TOF Bny #6 (32 Counts)	TOF Bny #5 (16 Counts)	TOF Bny #4 (8 Counts)	TOF Bny #3 (4 Counts)	TOF Bny #2 (2 Counts)	TOF Bny #1 (1 Count)
	MOST SIGNIFICANT BIT OF SA DATA				LEAST SIGNIFICANT BIT OF SA DATA	
Level B:	SA Bny #5 (16 Counts)	SA Bny #4 (8 Counts)	SA Bny #3 (4 Counts)	SA Bny #2 (2 Counts)	SA Bny #1 (1 Count)	Status/RFI Binary
	MOST SIGNIFICANT BIT OF M_T PHA		LEAST SIGNIF. BIT OF M_T PHA	MOST SIGNIF. BIT OF M_P PHA		LEAST SIGNIFICANT BIT OF M_P PHA
Level C:	M_T PHA Bny #3 (4 Counts)	M_T PHA Bny #2 (2 Counts)	M_T PHA Bny #1 (1 Count)	M_P PHA Bny #3 (4 Counts)	M_P PHA Bny #2 (2 Counts)	M_P PHA Bny #1 (1 Count)
	MOST SIGNIFICANT BIT OF M_T ACC		LEAST SIGNIF. BIT OF M_T ACC	MOST SIGNIF. BIT OF M_P ACC		LEAST SIGNIFICANT BIT OF M_P ACC
Level D:	M_T ACC Bny #3 (4 Counts)	M_T ACC Bny #2 (2 Counts)	M_T ACC Bny #1 (1 Count)	M_P ACC Bny #3 (4 Counts)	M_P ACC Bny #2 (2 Counts)	M_P ACC Bny #1 (1 Count)
	→ TIME →					

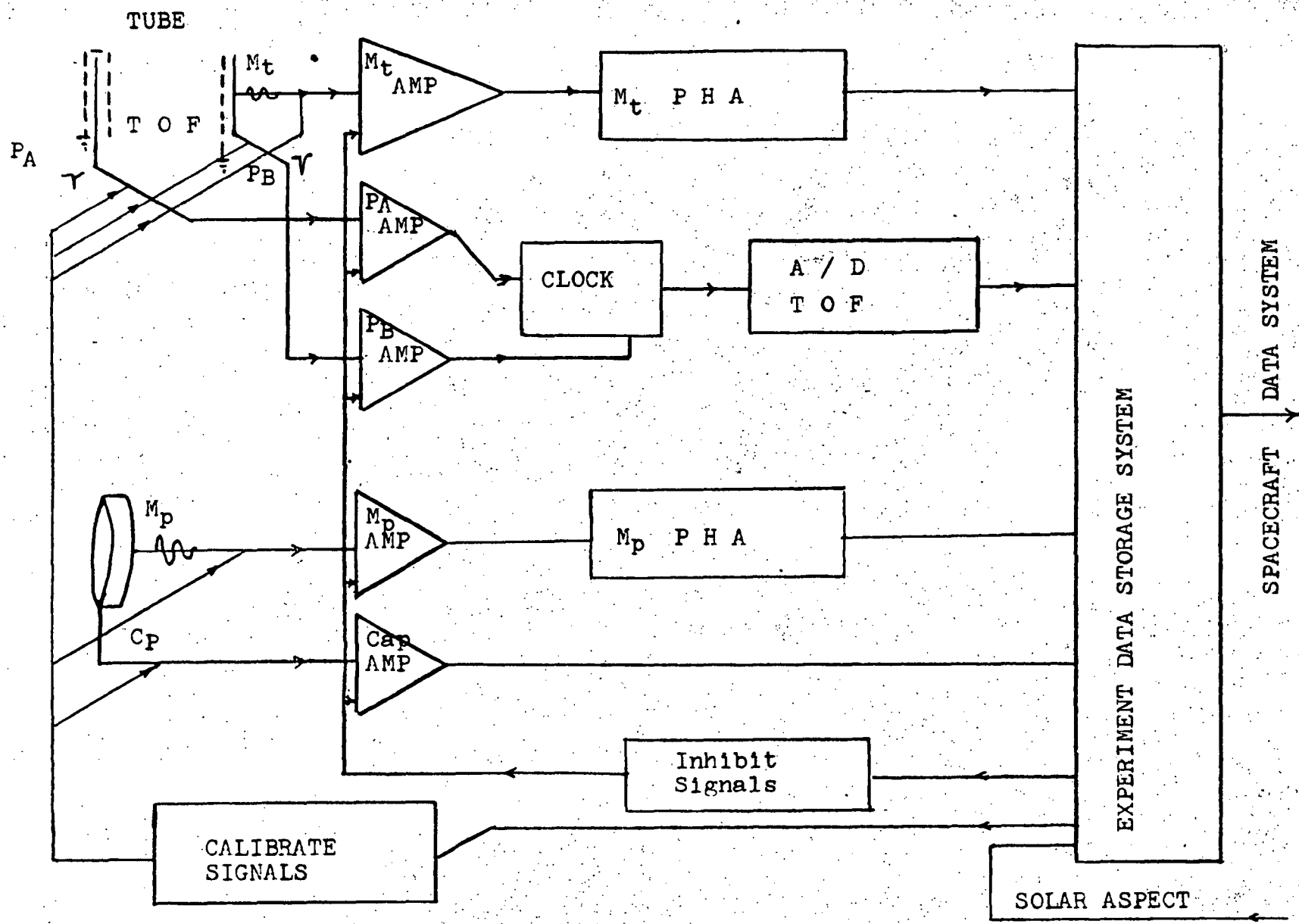

APPENDIX I FIG. 1

B

APPENDIX II

PAPERS AND PUBLICATIONS 1968-

1. "Zodiacal Dust: Measurements in Cis-Lunar and Interplanetary Space Between June and December 1966 from OGO III and Mariner IV", Space Research VIII, North-Holland Publishing Co., Amsterdam, 1968.

2. "Results of Recent Microparticle Hypervelocity Impact Studies Related to Sensors of Cosmic Dust Experiments", Space Research VIII, North-Holland Publishing Co., Amsterdam, 1968.

3. "Results of Studies of Thermal Gradient Effects on Ceramic Transducer Sensors Used in Cosmic Dust Experiments", Space Research VIII, North-Holland Publishing Co., Amsterdam, 1968.

4. "Lunar Explorer 35: Initial Measurements from the Cosmic Dust Experiment", Transactions American Geophysical Union, Volume 49, No. 1, P. 243, March, 1968.

5. "Mariner IV and OGO III: Temporal Variations of Dust Particle Flux in the Zodiacal Dust Cloud", Transactions American Geophysical Union, Volume 49, No. 4, p. 724, December 1968

6. "Mariner IV: Detection of Inspiraling Particles from Encke's Comet" Transactions American Geophysical Union, Volume 49, No. 4, P. 724, December, 1968.

7. "Lunar Explorer 35: Lunar Ejecta Related to Major Meteor Streams", Transactions American Geophysical Union, Volume 49, No. 4, p. 724, December, 1968.

8. "Lunar Explorer 35: Direct Measurements of Dust Particles in Selenocentric Space", 72nd Meeting of Texas Academy of Science, Abstract published by Texas Journal of Science, Spring, 1969.

9. "Analytical Studies of the Dynamics of Picogram Particles Ejected from the Lunar Surface", 72nd Meeting of Texas Academy of Science Abstract published by Texas Journal of Science, Spring, 1969.

10. "Lunar Explorer 35: Studies of the Relationship Between Lunar Ejecta Produced by Meteor Showers and Enhanced Dust Particle Flux in Selenocentric and Cis-Lunar Space", 72nd Meeting of Texas Academy of Science, Abstract Published by Texas Journal of Science, Spring, 1969.

11. "Investigation of the Flux of Picogram Dust Particles in the Geminid Meteor Stream from a Black Brant II Rocket Experiment", 72nd Meeting of Texas Academy of Science, Abstract published by Texas Journal of Science, Spring, 1969.

12. "Results of Studies of Poynting-Robertson Effect on Picogram Encke Comet Particles from Mariner IV Cosmic Dust Experiment Measurements", 72nd Meeting of Texas Academy of Science, Abstract published by Texas Journal of Science, Spring, 1969.

13. "Radiation Pressure and Drag Forces Acting on Picogram Interplanetary Dust Particles in Heliocentric Space", 72nd Meeting of Texas Academy of Science, Abstract published by Texas Journal of Science, Spring, 1969.

14. "Lunar Explorer 35: Picogram Lunar Ejecta Related to the Orionid and Leonid Meteor Showers, 1968 and 1969", Transactions, American Geophysical Union, Volume 50, No . 4, p. 222, April 1969.

15. "Lunar Explorer 35: Indications of Mass Limit for Lunar Ejecta Resulting from Hypervelocity Impact of Meteoroids on the Lunar Surface", Transactions, American Geophysical Union, Volume 50, No.4, p. 222, April 1969.

16. "Picogram Dust Particle Flux: 1967-1968 Measurements in Selenocentric Cislunar, Interplanetary Space," Space Research X, North-Holland Publishing Co., Amsterdam, 1968.

17. "Lunar Explorer 35: Dust Particle Measurements in Selenocentric Space During Periods of Meteor Showers of 1967-68-69.," Transactions, American Geophysical Union, Volume 51, No. 4, April 1970.

18. "Lunar Explorer 35: Dust Particle Measurements in Selenocentric Space During Periods of the Geninid Meteor Showers of 1967-68-69II," Transactions, American Geophysical Union, Volume 51, No. 11, November 1970, P. 769.

19. "Lunar Explorer 35 and OGO III: Dust Particle Measurements in Selenocentric and Cislunar Space from 1967 to 1969", Space Research XI Akademie-Verlag, Berlin, 1971.

20. "OGO III: Measured Speeds of Micron-sized Dust Particles in Cislunar Space." Transactions of the American Geophysical Union, Vol. 52, No. 4, April, 1971.

21. "Initial Results of a Microparticle Detection Experiment on A Rocket Launched During the 1970 Geminid Meteor Shower." Transactions of the American Geophysical Union, Vol, 52, No. 4, April, 1971

22. "Final Results of a 1970 Geminid Dust Particle Rocket Experiment," Transactions of the American Geophysical Union, Vol, 52, No. 11, November, 1971.

23. "Lunar Explorer 35: 1970 Dust Particle Data & Analysis of Shower Related Picogram Lunar Ejecta Orbits In the Earth-Moon Systems," Space Research XII, Akademie-Verlag, Berlin, 1972..

24. "Results of a 1970 Geminid Dust Particle Rocket Experiment and Analysis of OGO III Dust Particle Velocity Measurements," Space Research XII, Akademie-Verlag, Berlin, 1972..

25. "Lunar Explorer 35: Orbital Studies of Picogram Lunar Ejecta During Perseid Meteor Showers, 1967, '68, '69, and '70." Transactions of the American Geophysical Union, Vol. 53, No. 4, April 1972.

26. "Four Years of Dust Particle Measurements in Cislunar and Selenocentric Space from Lunar Explorer 35 and OGO III," Space Research XIII, Akademie-Verlag, Berlin, 1973.

27. "Review of Dust Particle Measurements from Satellites and Probes: 1958 - 1972," invited paper presented to the School of Physics, University of Newcastle upon Tyne, Newcastle, England. Abstract published in regional science news letter, February 1973.

28. "Developement of Curriculum for an Interdisciplinary Program in Environmental Education", invited paper presented to the faculty of all of the Schools of the Sciences at the University of Newcastle upon Tyne, Newcastle, England. February 1973.

29. "Lunar Explorer 35: Evidence of Lunar Ejecta Dyring Periods of Major Meteor Showers," invited paper presented at a meeting of the faculty and graduate students at University of Sheffield, Sheffield, England. February 1973.

30. "Lunar Explorer 35: Orbits of Lunar Ejecta in Selenocentric and Cis-Lunar Space," invited paper, National German Academy of Science meeting, Gutenberg, FRG, March, 1973. Abstract published in proceedings of the meeting.

31. "Comparisons of Satellite and Probe Measurements of Cosmic Dust and Results of Ground-based Zodiacal Light Experiments," invited paper presented to faculty and guest astronomers of Sweden at Lund Astronomical Observatory, Lund, Sweden, April, 1973.

32. "Comparisons of Pioneer 8 & 9 and Mariner IV Dust Particle Measurements Near 1 AU," invited paper presented to the National Swedish Space Council, Stockholm, Sweden, April 1973.

33. "Review of Mariner IV Cosmic Dust Measurement and Comparison With Preliminary Results of Pioneer 10," invited paper presented at Konstanz, Germany meeting of COSPAR, with abstract published in proceedings of the meeting, May, 1973.

34. "Mariner IV: A Study of the Cumlative Flux of Dust Particles Over a Heliocentric Range of 1 to 1.56 AU," Space Research XIV, Academie-Verlag, Berlin, 1974, in print.